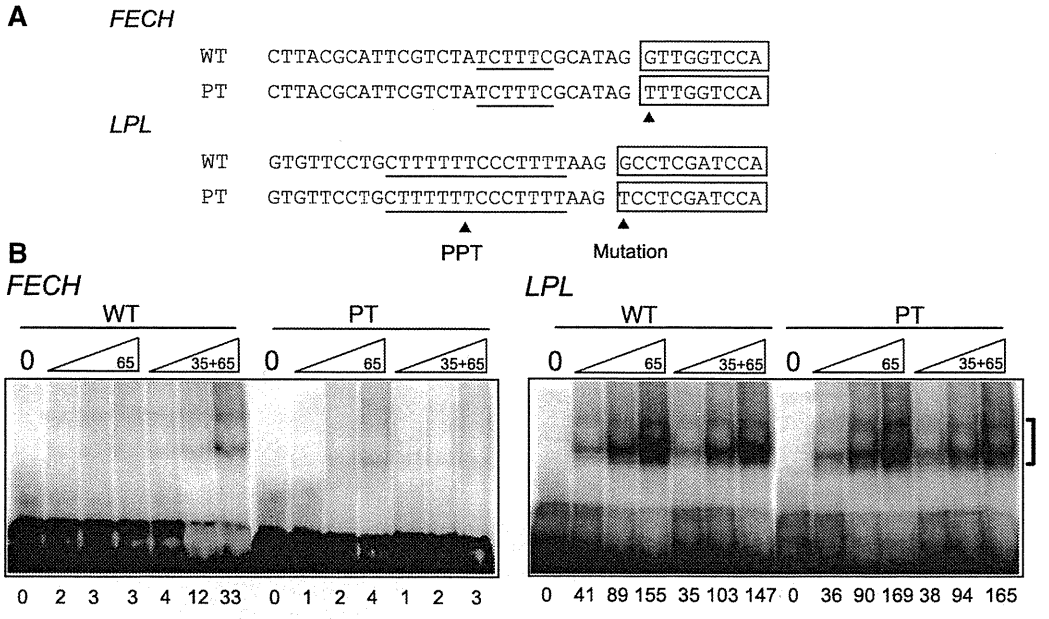

Figure 3. RNA-EMSA. (**A**) Sequences of wild-type (WT) and mutant (PT) RNA probes of *FECH* and *LPL* employed for RNA-EMSA. (**B**) RNA-EMSA of wild-type and mutant *FECH* and *LPL* with increasing amounts of $U2AF^{65}$ with or without $U2AF^{35}$. His-tagged $U2AF^{65}$ and $U2AF^{35}$ are expressed in Sf9 cells and are purified. Wild-type *FECH* requires $U2AF^{35}$ to bind to $U2AF^{65}$, whereas wild-type *LPL* does not require $U2AF^{35}$. A mutation at E^{+1} abrogates binding of $U2AF^{65}$ in *FECH* but not in *LPL*. Concentrations of $U2AF^{35}$ are 5, 10 and 20 ng/μl; and those of $U2AF^{65}$ are 10, 20 and 40 ng/μl. Numbers at the bottom indicate intensities of the retarded fragments in arbitrary units.

of $U2AF^{35}$ gained its binding. For the mutant *FECH*, neither $U2AF^{65}$ alone nor addition of both U2AFs showed binding of U2AFs. On the other hand, the wild-type *LPL* did not require $U2AF^{35}$ to bind to $U2AF^{65}$. Addition of $U2AF^{35}$ did not substantially increased binding of $U2AF^{65}$. These bindings were not affected by the mutation at E^{+1} of *LPL* (Figure 3B).

These results indicate that the mutation in *FECH* compromises a binding affinity for $U2AF^{35}$, which in turn abrogates binding of $U2AF^{65}$ and results in aberrant splicing. On the other hand, wild-type *LPL* does not need to bind to $U2AF^{35}$ and the mutation at E^{+1} has no effect on the assembly of spliceosome.

PPT determines the splicing consequences of the mutations

In an effort to delineate effects of the PPT sequences on the splicing consequence of a mutation at E^{+1}, we introduced a series of mutations into the PPT in the presence of the mutation at E^{+1}. Extensions of the polypyrimidine stretch ameliorated aberrant splicing in *GH1*, *FECH* and *EYA1*. Conversely, truncations or disruptions of the polypyrimidine stretch caused exon skipping in *LPL* and *HEXA* (Figure 4).

Length of the polypyrimidine stretch best predicts the splicing consequences

We next sought for parameters that differentiate normal and aberrant splicings in these minigenes. Analysis of parameters that potentially dictate the strength of the PPT indicated that the length of pyrimidine stretch, the number of pyrimidines in 25 or 50 nt at the 3′-end of an intron correlated with the ratio of exon skipping with correlation coefficients of more than 0.6 (Supplementary Table S1). The number of pyrimidines in 25 or 50 nt at the 3′-end of an intron, however, failed to predict splicing consequences of nine other constructs shown in Figure 6, and is likely to be overfitted parameters unique to the 35 constructs in Figure 4. Coolidge and colleagues report that $(GU)_{11}$ in PPT is partly functional, but we did not observe alternative purine and pyrimidine residues in our PPTs and did not quantify effects of alternative nucleotides (10). We thus took the length of pyrimidine stretch as a best parameter to dictate the strength of the PPT (Figure 5A). The native *GH1*, *FECH* and *EYA1* carry a stretch of 6–10 pyrimidines, whereas the native *LPL* and *HEXA* harbor a stretch of 14 and 13 pyrimidines, respectively (arrows in Figure 5A). For highly degenerate PPTs in the artificial constructs, the total number of pyrimidines in a stretch of 25 nt at the 3′-end of an intron well predicts the ratio of exon skipping (Figure 5B). These analyses revealed that the length of the polypyrimidine stretch should be at least 10–15 nt to ensure normal splicing even in the presence of a mutation at E^{+1}.

Identification of effects on pre-mRNA splicing of nine disease-associated mutations at the first nucleotide of an exon

We next examined other mutations at E^{+1} in which splicing consequences have not been previously analyzed. We first identified 224 mutations that abrogate the first 'G' nucleotide of an exon in the Human Gene Mutation Database at http://www.hgmd.cf.ac.uk/ (data not shown). Among these, we arbitrarily chose nine mutations causing

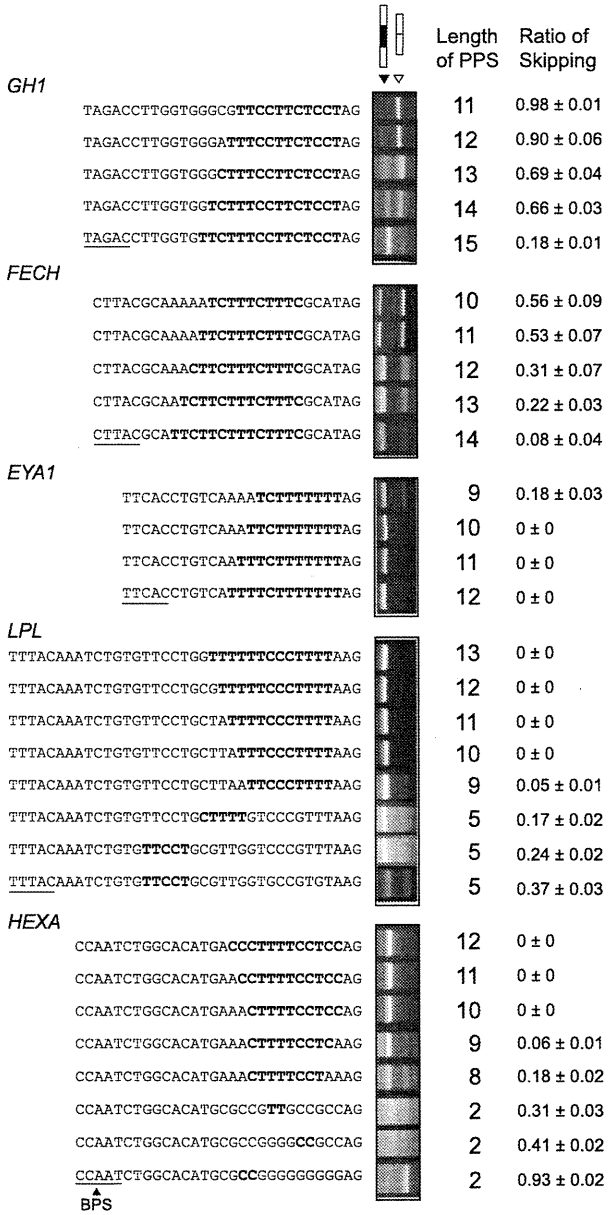

Figure 4. RT–PCR of HEK293 cells transfected with minigenes carrying artificially extended or disrupted PPT's. All the constructs harbor a mutation at E^{+1}. The top construct of each gene represents the patient's sequence. Only the nucleotide sequences of the 3′-end of an intron are indicated. The longest stretches of the polypyrimidines are shown in bold. Underlines indicate putative BPS's. The rightmost column shows the mean and SD of three independent experiments of the densitometric ratios of the exon-skipped product.

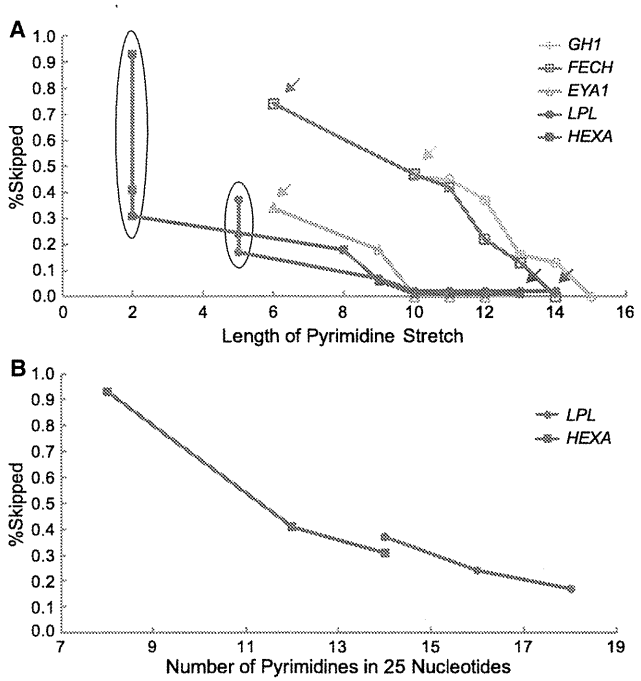

Figure 5. Ratios of exon skipping are plotted against the lengths of the polypyrimidine stretch (**A**) and the numbers of pyrimidines in 25 nt at the 3′-end of an intron (**B**). The ordinate (percent skipped) represents the ratios of exon skipping compared to that of the wild-type construct. The data are obtained from RT–PCR shown in Figure 4. Arrows indicate the original constructs carrying the patient's sequence, and the others are artificial constructs. Six constructs indicated by ovals in (A) are plotted in (B).

neuromuscular and musculoskeletal disorders (Figure 6A).

We constructed nine pairs of wild-type and mutant minigenes, and introduced them into HEK293 cells. We observed aberrant splicing in *PKHD1*, *COL1A2* (exon 37), *CLCN2*, *CAPN3* (exons 10 and 17), but not in *LAMA2*, *NEU1*, *COL6A2* and *COL1A2* (exon 23) (Figure 6B). The lengths of the polypyrimidine stretch of the five aberrantly spliced constructs ranged from 4 to 10 nt, whereas those of the four normally spliced constructs ranged from 9 to 16 nt. These results are in concordance with a notion that the short polypyrimidine stretches are predisposed to aberrant splicing due to a mutation at E^{+1}, whereas long polypyrimidine stretches are tolerant to such mutations. Among the 224 mutations affecting 'G' at E^{+1}, only three mutations have been reported to cause aberrant splicing. We here analyzed nine mutations and identified five more such mutations. It is thus likely that most splicing mutations at E^{+1} still remain unrecognized to date.

Analysis of the 3′-splice sites of the human genome

We next analyzed PPTs of 176 809 introns of the entire human genome. The length of the pyrimidine stretch was shorter when E^{+1} was the conserved 'G' (Figure 7A). This also supports a notion that AG-dependent 3′ ss harboring G at E^{+1} has a short polypyrimidine stretch (12). In addition, the ratio of 'C' at intronic position −3 was lower when E^{+1} was the conserved 'G' (Figure 7B), which suggests that G at E^{+1} makes C at −3 dispensable for binding to U2AF[35], although this is not directly relevant to the length of the PPT.

Being prompted by a previous report that U2AF[35] binds up to the 10th nucleotide of an exon (12), we examined nucleotide frequencies at exonic positions +1

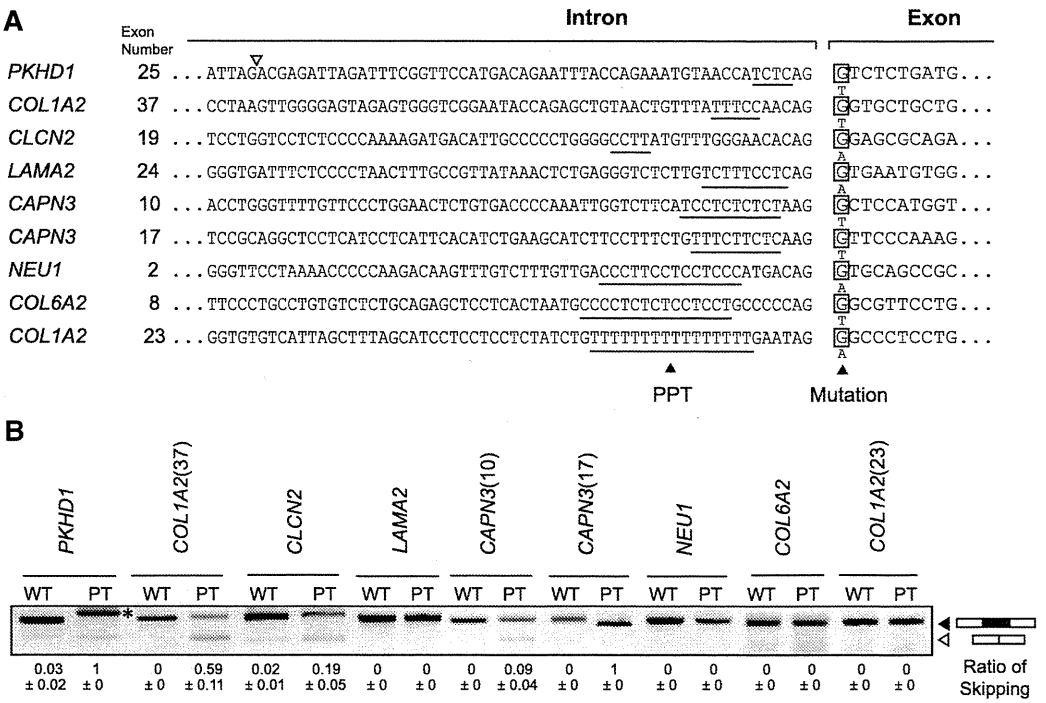

Figure 6. RT–PCR analysis of nine disease-causing mutations at E^{+1}. (**A**) Sequences at the intron/exon junctions of nine pairs of wild-type and mutant constructs. The longest polypyrimidine stretches are underlined. (**B**) RT–PCR of minigenes transfected into HEK293 cells. Five mutant constructs are aberrantly spliced, whereas the remaining four mutants are normally spliced. Numbers in the parentheses indicate exon numbers. In *PKHD1*, a cryptic 3′-splice site (open arrowhead in panel A) at 55 nt upstream of the native site is activated (asterisk). Mean and SD of three independent experiments of the densitometric ratios of the exon-skipped product is shown at the bottom.

to +12. We counted only wobbling nucleotides based on the human genome annotation NCBI Build 37.1 (hg19). As expected, 'GT' dinucleotide was frequently observed at exonic positions +1 and +2. We also observed preference for a 'T' nucleotide at positions +3 to +5 (Figure 7C). Alignment of SELEX results of $U2AF^{35}$ by Wu and colleagues (12) similarly demonstrate overrepresentation of 'T' nucleotides at positions +3 to +6 (Figure 7D). We thus analyzed effects of 'TTT' at positions +3 to +5 using the *GH1, FECH* and *EYA1* minigenes carrying the patient's mutations. We found that introduction of 'TTT' at exonic position +3 to +5 had no effect in *GH1* and *FECH*, but slightly enhanced exon recognition in *EYA1* (Figure 7E).

DISCUSSION

We previously reported that the SD-score algorithm efficiently predicts splicing consequences of a mutation affecting the 5′ ss (32). We next identified that the human BPS consensus is simply yUnAy (5), and hoped to predict if a given mutation affecting the BPS causes aberrant splicing or not. The high degeneracy of the BPS consensus, however, prevented us from constructing an efficient algorithm. In this communication, we worked on mutations at E^{+1}. As far as we know, only three such mutations have been reported to cause aberrant splicing, and only two such mutations have been reported not to affect splicing. Knockdown and RNA-EMSA of $U2AF^{35}$, as well as analyses of artificial PPT mutations and nine disease-causing mutations at E^{+1} revealed that AG-dependence of 3′ ss determines the splicing consequences. In the presence of a mutation at E^{+1}, a stretch of 15 or more pyrimidines ensures normal splicing, whereas a stretch of 10 or less pyrimidines are predisposed to aberrant splicing.

AG-dependent 3′ ss requires both $U2AF^{65}$ and $U2AF^{35}$ to bring U2snRNP to the branch point, whereas AG-independent 3′ ss has a long stretch of pyrimidines that can bind to $U2AF^{65}$ without $U2AF^{35}$ (13,15). $U2AF^{35}$ potentially provides an additional RNA–protein interacting force and an additional SR protein-binding surfaces (33). An artificial G-to-C mutation at E^{+1} downstream of a stretch of five pyrimidines in the mouse IgM gene abrogates binding of $U2AF^{35}$ and causes defective splicing (14). Similarly, in *INSR* exon 11 carrying an 'A' nucleotide at E^{+1}, a stretch of 14 pyrimidines but not of 10 pyrimidines is properly spliced (34). Additionally, a stretch of eight pyrimidines upstream of the last exon with 'C' at E^{+1} of *EIF3S7* is dependent on $U2AF^{35}$, whereas a stretch of 14 pyrimidines upstream of the last exon with 'A' at E^{+1} of *CUEDC1* is independent (15). Our observations and previous reports all point to a notion that effects on pre-mRNA splicing should be scrutinized for a mutation at E^{+1} if the preceding intron carries a short stretch of 10 or less pyrimidines. Indeed, in our analysis of nine disease-causing mutations, five of six mutants with 10 or less contiguous pyrimidines were aberrantly spliced (Figure 6), but no splicing analysis has been documented for any of them.

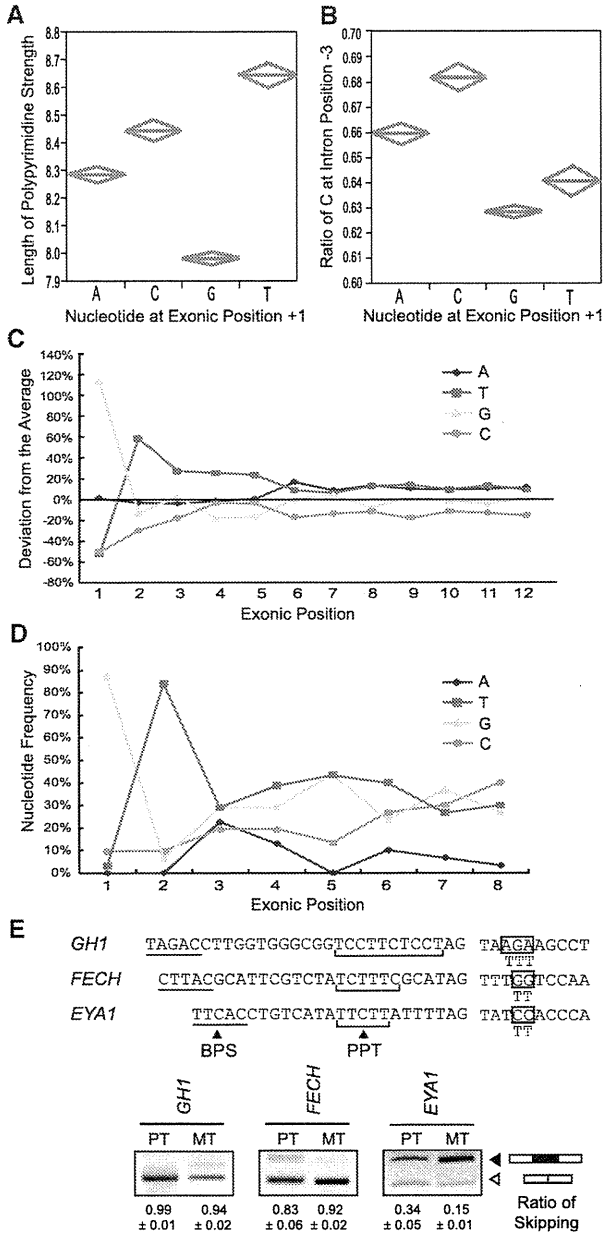

Figure 7. (**A**) Polypyrimidine stretch and the first nucleotide of an exon in the human genome. The longest stretch of uninterrupted pyrimidines among 25 nt at the 3′-ends of an intron is counted for 176 809 introns of the human genome. Diamonds represent means and 95% confidence intervals. One-way ANOVA and Fisher's-multiple range test revealed statistical significance of $P < 0.0001$. (**B**) Ratios of 'C' at position −3 in relation to the first nucleotide of an exon are analyzed for 176 809 introns of the human genome. Diamonds represent means and 95% confidence intervals. One-way ANOVA and Fisher's-multiple range test revealed statistical significance of $P < 0.0001$. (**C**) Preferentially observed nucleotides at the 5′-end of an exon in human. Only wobbling nucleotides are counted in the human genome. (**D**) Nucleotide frequencies at exonic positions +1 to +8 according to the SELEX data of U2AF^{35} by Wu and colleagues (12). (**E**) Effects of 'TTT' at exonic positions +3 to +5 in *GH1*, *FECH* and *EYA1* carrying the patient's mutation at E^{+1}. Artificially substituted exonic nucleotides are indicated by boxes. Mean and SD of three independent experiments of the densitometric ratios of the exon-skipped product is shown at the bottom.

We first report overrepresentation of 'T' nucleotides at exonic positions +3 to +5 in the human genome, as well as in *in vitro* U2AF^{35}-binding sites. Enhancement of exon recognition in *EYA1* by introduction of 'TTT' at positions +3 to +5 also underscores a notion that 'TTT' at +3 to +5 is likely to enhance binding of U2AF^{35}. Effects of 'TTT', however, were not observed in *GH1* and *FECH*. As the patient's mutation in *GH1* and *FECH* resulted in almost complete skipping of an exon, whereas that in *EYA1* gave rise to both exon-skipped and included products. The degrees of aberration of exon recognition may account for the 'TTT'-responsiveness. Alternatively, although no ESE motif was detected in the 'TTT'-introduced *EYA1* by five different ESE search tools, an unrecognized ESE might have ameliorated exon skipping in *EYA1*. Further analysis is required to elucidate effects of overrepresentation of 'T' at positions +3 to +5.

SUPPLEMENTARY DATA

Supplementary Data are available at NAR Online.

FUNDING

Grants-in-Aids from the Ministry of Education, Culture, Sports, Science and Technology of Japan; Ministry of Health, Labor and Welfare of Japan. Funding for open access charge: Innovative Cell Biology by Innovative Technology granted by the Japan Science and Technology Agency (JST).

Conflict of interest statement. None declared.

REFERENCES

1. Black,D.L. (2003) Mechanisms of alternative pre-messenger RNA splicing. *Annu. Rev. Biochem.*, **72**, 291–336.
2. Jurica,M.S. and Moore,M.J. (2003) Pre-mRNA splicing: awash in a sea of proteins. *Mol. Cell*, **12**, 5–14.
3. Reed,R. (1996) Initial splice-site recognition and pairing during pre-mRNA splicing. *Curr. Opin. Gen. Dev.*, **6**, 215–220.
4. Parker,R., Siliciano,P.G. and Guthrie,C. (1987) Recognition of the TACTAAC box during mRNA splicing in yeast involves base pairing to the U2-like snRNA. *Cell*, **49**, 229–239.
5. Gao,K., Masuda,A., Matsuura,T. and Ohno,K. (2008) Human branch point consensus sequence is yUnAy. *Nucleic Acids Res.*, **36**, 2257–2267.
6. Zorio,D.A. and Blumenthal,T. (1999) Both subunits of U2AF recognize the 3′ splice site in Caenorhabditis elegans. *Nature*, **402**, 835–838.
7. Merendino,L., Guth,S., Bilbao,D., Martinez,C. and Valcarcel,J. (1999) Inhibition of msl-2 splicing by Sex-lethal reveals interaction between U2AF35 and the 3′ splice site AG. *Nature*, **402**, 838–841.
8. Kielkopf,C.L., Rodionova,N.A., Green,M.R. and Burley,S.K. (2001) A novel peptide recognition mode revealed by the X-ray structure of a core U2AF35/U2AF65 heterodimer. *Cell*, **106**, 595–605.
9. Mullen,M.P., Smith,C.W., Patton,J.G. and Nadal-Ginard,B. (1991) Alpha-tropomyosin mutually exclusive exon selection: competition between branchpoint/polypyrimidine tracts determines default exon choice. *Genes Dev.*, **5**, 642–655.
10. Coolidge,C.J., Seely,R.J. and Patton,J.G. (1997) Functional analysis of the polypyrimidine tract in pre-mRNA splicing. *Nucleic Acids Res.*, **25**, 888–896.

11. Soares,L.M., Zanier,K., Mackereth,C., Sattler,M. and Valcarcel,J. (2006) Intron removal requires proofreading of U2AF/3′ splice site recognition by DEK. *Science*, **312**, 1961–1965.
12. Wu,S., Romfo,C.M., Nilsen,T.W. and Green,M.R. (1999) Functional recognition of the 3′ splice site AG by the splicing factor U2AF35. *Nature*, **402**, 832–835.
13. Guth,S., Martinez,C., Gaur,R.K. and Valcarcel,J. (1999) Evidence for substrate-specific requirement of the splicing factor U2AF(35) and for its function after polypyrimidine tract recognition by U2AF(65). *Mol. Cell. Biol.*, **19**, 8263–8271.
14. Guth,S., Tange,T.O., Kellenberger,E. and Valcarcel,J. (2001) Dual function for U2AF(35) in AG-dependent pre-mRNA splicing. *Mol. Cell. Biol.*, **21**, 7673–7681.
15. Pacheco,T.R., Coelho,M.B., Desterro,J.M., Mollet,I. and Carmo-Fonseca,M. (2006) In vivo requirement of the small subunit of U2AF for recognition of a weak 3′ splice site. *Mol. Cell. Biol.*, **26**, 8183–8190.
16. Vorechovsky,I. (2006) Aberrant 3′ splice sites in human disease genes: mutation pattern, nucleotide structure and comparison of computational tools that predict their utilization. *Nucleic Acids Res.*, **34**, 4630–4641.
17. Lefevre,S.H., Chauveinc,L., Stoppa-Lyonnet,D., Michon,J., Lumbroso,L., Berthet,P., Frappaz,D., Dutrillaux,B., Chevillard,S. and Malfoy,B. (2002) A T to C mutation in the polypyrimidine tract of the exon 9 splicing site of the RB1 gene responsible for low penetrance hereditary retinoblastoma. *J. Med. Genet.*, **39**, E21.
18. Faustino,N.A. and Cooper,T.A. (2003) Pre-mRNA splicing and human disease. *Genes Dev.*, **17**, 419–437.
19. Wang,X.-H., Poh-Fitzpatrick,M., Chen,T., Malavade,K., Carriero,D. and Piomelli,S. (1995) Systematic screening for RNA with skipped exons - splicing mutations of the ferrochelatase gene. *Biochim. Biophys. Acta*, **1271**, 358–362.
20. Takahashi,I., Takahashi,T., Komatsu,M., Sato,T. and Takada,G. (2002) An exonic mutation of the GH-1 gene causing familial isolated growth hormone deficiency type II. *Clin. Genet.*, **61**, 222–225.
21. Okada,K., Inoue,A., Okada,M., Murata,Y., Kakuta,S., Jigami,T., Kubo,S., Shiraishi,H., Eguchi,K., Motomura,M. *et al.* (2006) The muscle protein Dok-7 is essential for neuromuscular synaptogenesis. *Science*, **312**, 1802–1805.
22. Ikeda,Y., Takagi,A., Nakata,Y., Sera,Y., Hyoudou,S., Hamamoto,K., Nishi,Y. and Yamamoto,A. (2001) Novel compound heterozygous mutations for lipoprotein lipase deficiency. A G-to-T transversion at the first position of exon 5 causing G154V missense mutation and a 5′ splice site mutation of intron 8. *J. Lipid Res.*, **42**, 1072–1081.
23. Petroulakis,E., Cao,Z., Clarke,J.T., Mahuran,D.J., Lee,G. and Triggs-Raine,B. (1998) W474C amino acid substitution affects early processing of the alpha-subunit of beta-hexosaminidase A and is associated with subacute G(M2) gangliosidosis. *Hum. Mutat.*, **11**, 432–442.
24. Kralovicova,J. and Vorechovsky,I. (2010) Allele-specific recognition of the 3′ splice site of INS intron 1. *Hum. Genet.*, **128**, 383–400.
25. Cartegni,L., Wang,J., Zhu,Z., Zhang,M.Q. and Krainer,A.R. (2003) ESEfinder: a web resource to identify exonic splicing enhancers. *Nucleic Acids Res.*, **31**, 3568–3571.
26. Smith,P.J., Zhang,C., Wang,J., Chew,S.L., Zhang,M.Q. and Krainer,A.R. (2006) An increased specificity score matrix for the prediction of SF2/ASF-specific exonic splicing enhancers. *Hum. Mol. Genet.*, **15**, 2490–2508.
27. Fairbrother,W.G., Yeh,R.F., Sharp,P.A. and Burge,C.B. (2002) Predictive identification of exonic splicing enhancers in human genes. *Science*, **297**, 1007–1013.
28. Wang,Z., Rolish,M.E., Yeo,G., Tung,V., Mawson,M. and Burge,C.B. (2004) Systematic identification and analysis of exonic splicing silencers. *Cell*, **119**, 831–845.
29. Zhang,X.H. and Chasin,L.A. (2004) Computational definition of sequence motifs governing constitutive exon splicing. *Genes Dev.*, **18**, 1241–1250.
30. Zhang,X.H., Kangsamaksin,T., Chao,M.S., Banerjee,J.K. and Chasin,L.A. (2005) Exon inclusion is dependent on predictable exonic splicing enhancers. *Mol. Cell. Biol.*, **25**, 7323–7332.
31. Goren,A., Ram,O., Amit,M., Keren,H., Lev-Maor,G., Vig,I., Pupko,T. and Ast,G. (2006) Comparative analysis identifies exonic splicing regulatory sequences–the complex definition of enhancers and silencers. *Mol. Cell*, **22**, 769–781.
32. Sahashi,K., Masuda,A., Matsuura,T., Shinmi,J., Zhang,Z., Takeshima,Y., Matsuo,M., Sobue,G. and Ohno,K. (2007) In vitro and in silico analysis reveals an efficient algorithm to predict the splicing consequences of mutations at the 5′ splice sites. *Nucleic Acids Res.*, **35**, 5995–6003.
33. Graveley,B.R. (2001) Alternative splicing: increasing diversity in the proteomic world. *Trends Genet.*, **17**, 100–107.
34. Kosaki,A., Nelson,J. and Webster,N.J. (1998) Identification of intron and exon sequences involved in alternative splicing of insulin receptor pre-mRNA. *J. Biol. Chem.*, **273**, 10331–10337.

Anti-MuSK autoantibodies block binding of collagen Q to MuSK

Y. Kawakami, BSc
M. Ito, PhD
M. Hirayama, MD, PhD
K. Sahashi, MD, PhD
B. Ohkawara, PhD
A. Masuda, MD, PhD
H. Nishida, MD, PhD
N. Mabuchi, MD, PhD
A.G. Engel, MD
K. Ohno, MD, PhD

Address correspondence and reprint requests to Dr. Ohno, Division of Neurogenetics, Center for Neurological Diseases and Cancer, Nagoya University Graduate School of Medicine, 65 Tsurumai, Showa-ku, Nagoya 466-8550, Japan
ohnok@med.nagoya-u.ac.jp

ABSTRACT

Objective: Muscle-specific receptor tyrosine kinase (MuSK) antibody-positive myasthenia gravis (MG) accounts for 5%–15% of autoimmune MG. MuSK mediates the agrin-signaling pathway and also anchors the collagenic tail subunit (ColQ) of acetylcholinesterase (AChE). The exact molecular target of MuSK-immunoglobulin G (IgG), however, remains elusive. As acetylcholine receptor (AChR) deficiency is typically mild and as cholinesterase inhibitors are generally ineffective, we asked if MuSK-IgG interferes with binding of ColQ to MuSK.

Methods: We used 3 assays: in vitro overlay of the human ColQ-tailed AChE to muscle sections of *Colq*−/− mice; in vitro plate-binding assay to quantitate binding of MuSK to ColQ and to LRP4; and passive transfer of MuSK-IgG to mice.

Results: The in vitro overlay assay revealed that MuSK-IgG blocks binding of ColQ to the neuromuscular junction. The in vitro plate-binding assay showed that MuSK-IgG exerts a dose-dependent block of MuSK binding to ColQ by but not to LRP4. Passive transfer of MuSK-IgG to mice reduced the size and density of ColQ to ~10% of controls and had a lesser effect on the size and density of AChR and MuSK.

Conclusions: As lack of ColQ compromises agrin-mediated AChR clustering in *Colq*−/− mice, a similar mechanism may lead to AChR deficiency in MuSK-MG patients. Our experiments also predict partial AChE deficiency in MuSK-MG patients, but AChE is not reduced in biopsied NMJs. In humans, binding of ColQ to MuSK may be dispensable for clustering ColQ, but is required for facilitating AChR clustering. Further studies will be required to elucidate the basis of this paradox. ***Neurology*® 2011;77:1819–1826**

GLOSSARY

AChE = acetylcholinesterase; **AChR** = acetylcholine receptor; **ColQ** = collagen Q; **IgG** = immunoglobulin G; **LRP4** = low-density lipoprotein receptor-related protein 4; **MG** = myasthenia gravis; **MuSK** = muscle-specific receptor tyrosine kinase; **NMJ** = neuromuscular junction; **SDS-PAGE** = sodium dodecyl sulfate-polyacrylamide gel electrophoresis.

During development of the neuromuscular junction (NMJ), neural agrin released from the nerve terminal binds to the postsynaptic transmembrane protein LRP4.[1,2] Dimerized LRP4 forms a heterotetramer with the dimerized muscle-specific receptor tyrosine kinase (MuSK).[3] MuSK together with Dok-7 promotes clustering of acetylcholine receptor (AChR) on the junctional folds by rapsyn.[4] The clustering effect of MuSK is mediated by distinct pathways involving Rho GTPase.[5]

Editorial, page 1783

At the NMJ, 3 tetramers of catalytic subunits of acetylcholinesterase (AChE) are linked to ColQ, the triple helical collagenic subunit.[6] ColQ-tailed AChE is anchored to the synaptic basal lamina by 2 mechanisms: 2 sets of heparan sulfate proteoglycan residues in the collagen

Supplemental data at www.neurology.org

Supplemental Data

From the Division of Neurogenetics (Y.K., M.I., B.O., A.M., K.O.), Center for Neurological Diseases and Cancer, Nagoya University Graduate School of Medicine, Nagoya; Department of Pathophysiological Laboratory Sciences (M.H.), Nagoya University Graduate School of Medicine, Nagoya; Department of Neurology (K.S.), Aichi Medical University, Aichi; Department of Neurology (H.N.), Gifu Prefectural General Medical Center, Gifu; Department of Neurology (N.M.), Okazaki City Hospital, Okazaki, Japan; and Department of Neurology (A.G.E.), Mayo Clinic, Rochester, MN.

Study funding: Supported by a Grant-in-Aid from the Ministry of Education, Culture, Sports, Science, and Technology of Japan; a Grant-in-Aid from the Ministry of Health, Labor, and Welfare of Japan; a research grant from the National Institute of Neurological Disorders and Stroke (NS6277); and a research grant from the Muscular Dystrophy Association.

Disclosure: Author disclosures are provided at the end of the article.

domain of ColQ[7] bind to heparin sulfate proteoglycans, such as perlecan[8]; and the C-terminal domain of ColQ binds to MuSK.[9]

Five percent to 15% of patients with myasthenia gravis (MG) carry antibodies against MuSK (MuSK–immunoglobulin G [IgG]).[10,11] MuSK-MG patients respond favorably to immunotherapy, but usually do not respond to, or are even worsened by, cholinesterase inhibitors.[12–15] Anti-AChR antibodies comprise IgG1 and IgG3 moieties that bind complement whereas anti-MuSK antibodies are largely IgG4 that do not activate complement, and complement deposits at the NMJ are sparse.[16–18] However, the exact target of MuSK-IgG remains elusive. We therefore examined an effect of MuSK-IgG on an interaction between ColQ and MuSK by in vitro and in vivo assays, and found that MuSK-IgG blocks this interaction.

METHODS

Patients. We obtained serum from 4 MuSK-MG patients (patients 1–4) and a patient with limb-girdle muscular dystrophy as a control (control 1). We obtained 10 mL peripheral blood from patients 1, 3, 4, and control and residual plasmapheresis fluid from patient 2. We also obtained expired fresh-frozen plasma (control 2) from Dr. Isao Takahashi at the Aichi Red Cross Blood Center with institutional approval. We used sera of patient 2 and control 2 for all the experiments, and sera of patients 1, 3, 4, and control 1 only for the in vitro overlay and in vitro plate binding assays because only small amounts of sera were available from these patients.

Ages and genders of patients 1–4 were a 48-year-old woman, a 30-year-old woman, a 59-year-old man, and a 45-year-old woman, respectively. The titers of anti-MuSK antibodies of patients 1–3 were 22.0 nM, 11.2 nM, and 0.12 nM, respectively (normal <0.01 nM). Patient 4 was positive for anti-MuSK antibody, but the titer was not determined.

Standard protocol approvals, registrations, and patient consents. We performed all human studies under the institutional review board approvals of the Nagoya University Graduate School of Medicine and the Mayo Clinic, and obtained written informed consents from each patient and a control. We also obtained approvals of the *Colq*−/− mice studies and the passive IgG transfer studies by the Animal Care and Use Committee of the Nagoya University.

Plasmids. We previously made CMV-based mammalian expression vectors, pTargeT-*COLQ* and pTargeT-*ACHE*.[19] To generate hMuSKect-myc, we cloned the extracellular domain (aa 1–393) of human *MUSK* cDNA (Open Biosystems) into a mammalian expression vector pAPtag-5 (GenHunter) at the *Nhe*I and *Xho*I sites upstream of a myc epitope. For hLRP4N-FLAG, we cloned the extracellular domain (aa 1–1722) of human *LRP4* cDNA (Open Biosystems) into the *Hin*dIII and *Xba*I sites upstream of a 3xFLAG epitope of a mammalian expression vector p3XFLAG-CMV-14 (Sigma Aldrich).

Preparation of recombinant human ColQ-tailed AChE. We prepared human ColQ-tailed AChE for in vitro overlay assay and for in vitro plate-binding assay. Both pTargeT-*COLQ* and pTargeT-*ACHE* were transfected into HEK293 cells in a 10-cm dish using the calcium phosphate method as described elsewhere.[20] We extracted proteins from the cells in Tris-HCl buffer (50 mM Tris-HCl [pH 7.0], 0.5% Triton X-100, 0.2 mM EDTA, leupeptin [2 μg/mL], and pepstatin [1 μg/mL]) containing 1 M NaCl, and diluted the extracts containing ColQ-tailed AChE in Tris-HCl buffer containing 0.2 M NaCl and loaded onto the HiTrap Heparin HP columns (GE Healthcare). We washed the columns with 5 volumes of Tris-HCl buffer containing 0.2 M NaCl, and eluted ColQ-tailed AChE with Tris-HCl buffer containing 1 M NaCl. We concentrated the eluate with an Amicon Ultra-4 Centrifugal Filter (50K) (Millipore) to 12-Ellman units per mL. The units were normalized with the Torpedo-derived AChE (C2888, Sigma-Aldrich).

Preparation of hMuSKect-myc and hLRP4N-FLAG proteins. We prepared hMuSKect-myc and hLRP4N-FLAG for in vitro plate-binding assays. We introduced a construct carrying either hMuSKect-myc or hLRP4N-FLAG into HEK293 cells in a 10-cm dish using the calcium phosphate method as above. We purified the hMuSKect-myc with the c-myc-Tagged Protein Mild Purification Kit version 2 (MBL), and purified the hLRP4N-FLAG with the Anti-DYKDDDDK-tag Antibody Beads (Wako). We detected purified hMuSKect-myc and hLRP4N-FLAG by anti-myc antibody (9E10, Abcam) and anti-FLAG antibody (M2, Sigma-Aldrich), respectively (data not shown), and also detected hMuSKect-myc by sodium dodecyl sulfate–polyacrylamide gel electrophoresis (SDS-PAGE) followed by protein staining with the Oriole Fluorescent Gel Stain (Bio-Rad).

Purification of plasma IgG. We purified IgG as described elsewhere[21] with minor modifications. We adjusted plasma to pH 8.0 with 1 M NaOH. While stirring 1 volume of plasma, we slowly added 3.5 volumes of 0.4% rivanol (Tokyo Chemical Industries) in water for 30 minutes. We left the solution overnight at RT, and removed a tenacious yellow precipitate. After filtering the supernatant through Whatman no. 1 paper to remove residual precipitates, we added 8 g of activated charcoal (Wako Chemicals) for 100 mL of the IgG solution and incubated overnight at 4°C to remove rivanol. We then slowly added an equal amount of saturated ammonium sulfate, and again incubated overnight at RT to precipitate crude IgG. We centrifuged the solution at 3,000 × *g* for 30 minutes, and added saline to the precipitate to form a slurry, which was then transferred to a dialysis tube (Spectra/Por MWCO 50,000, Spectrum Laboratories). We dialyzed the solution in saline at 4°C for 3 hours, followed by dialysis in PBS at 4°C for 2 hours and then overnight. We removed residual charcoals by filtering through a 0.22-μm Millex-GP filter (Millipore), and concentrated IgG using Amicon Ultra 50K (Millipore). We confirmed purity of isolated IgG by 6% SDS-PAGE under a nonreducing condition. We also reduced IgG in 4% 2-mercaptoethanol and fractionated the heavy and light chains by 10% SDS-PAGE.

Incubation of purified IgG to a muscle section of *Colq*−/− mice. We prepared 10-μm-thick sections of quadriceps muscles of *Colq*−/− mice[22] with a Leica CW3050–4 cryostat at −20°C. We blocked nonspecific binding of a muscle section with the blocking buffer that contained 5% sheep serum in PBS at RT for 2 hours. We suspended the purified IgG in the blocking buffer at 50 μg/mL, and overlaid it on a muscle section at 4°C overnight. We detected human IgG by FITC-labeled

anti-human IgG antibody (02–10-06, KPL), and AChR by Alexa594-labeled α-bungarotoxin (Molecular Probes).

In vitro overlay assay. The overlay binding method was essentially as previously described.[23] We overlaid 600 μg IgG of patients at 4°C overnight before adding 120-milli-Ellman units of ColQ-tailed AChE.

In vitro plate-binding assay for quantifying ColQ-MuSK interaction. We coated the Maxi-Sorp Immuno Plate (Nunc) with 0.15 μg of purified hMuSKect-myc at 4°C overnight and then incubated it with a blocking buffer that contained 50 mM Tris-HCl (pH 7.4), 0.5% BSA, 0.5% ovalbumin, and 0.5 M NaCl at RT for 1 hour. We incubated the wells with 1 pg to 100 μg of IgG of controls 1 and 2 and patients 1–4 at 4°C for 6 hours. We added 0.12-Ellman units of ColQ-tailed AChE as described above. We then quantified the bound ColQ-tailed AChE by the Ellman method in the presence of 5×10^{-5} M ethopropazine.[19] Each time before we moved to the next step, we washed the plate 3 times with PBS.

In vitro plate-binding assay for quantifying LRP4-MuSK interaction. We coated the Maxi-Sorp Immuno Plate with 0.15 μg of purified hMuSKect-myc as described above, and then blocked with 1% BSA in PBS at RT for 1 hour. We incubated the wells with 1 pg to 100 μg of IgG of control 2 and patient 2 at 4°C for 6 hours. We added 0.12 μg of purified hLRP4N-FLAG on each well at RT for 2 hours. We then quantified the bound hLRP4N-FALG by anti-FLAG-HRP using the TMB substrate kit (Pierce). Again, between each step, we washed the plates 3 times with PBS.

Passive transfer of human IgG to mice. We made passive transfer model mice as described elsewhere.[24] We intraperitoneally injected 40 mg IgG of control 2 and patient 2 into 6-week-old female C57BL/6J mice every day for 15 days. We sterilized IgG with a 0.22-μm filter (Millipore) and dissolved it in 400 μL PBS. The mice were killed on day 16 under deep anesthesia. To suppress any active immune response to the human protein,[25] we injected 300 mg/kg of cyclophosphamide monohydrate (10 mg/mL in 0.9% NaCl) intraperitoneally 24 hours after the first IgG injection. We also injected IgG of patient 2 into 2 additional mice to confirm consistency, and analyzed a representative mouse in detail. We detected AChR by Alexa594-labeled α-bungarotoxin (Molecular Probes), ColQ by 1:100 of a newly raised anti-ColQ antibody (figure e-1 on the *Neurology*® Web site at www.neurology.org), and MuSK by 1:100 of anti-MuSK antibody (C-19, Santa Cruz). We quantified signals by the BZ-9000 microscope (Keyence) equipped with the Dynamic Cell Count software BZ-H1C (Keyence).

Figure 1 **Muscle-specific receptor tyrosine kinase (MuSK)-immunoglobulin G (IgG) recognizes the neuromuscular junction (NMJ) of *Colq*−/− mice**

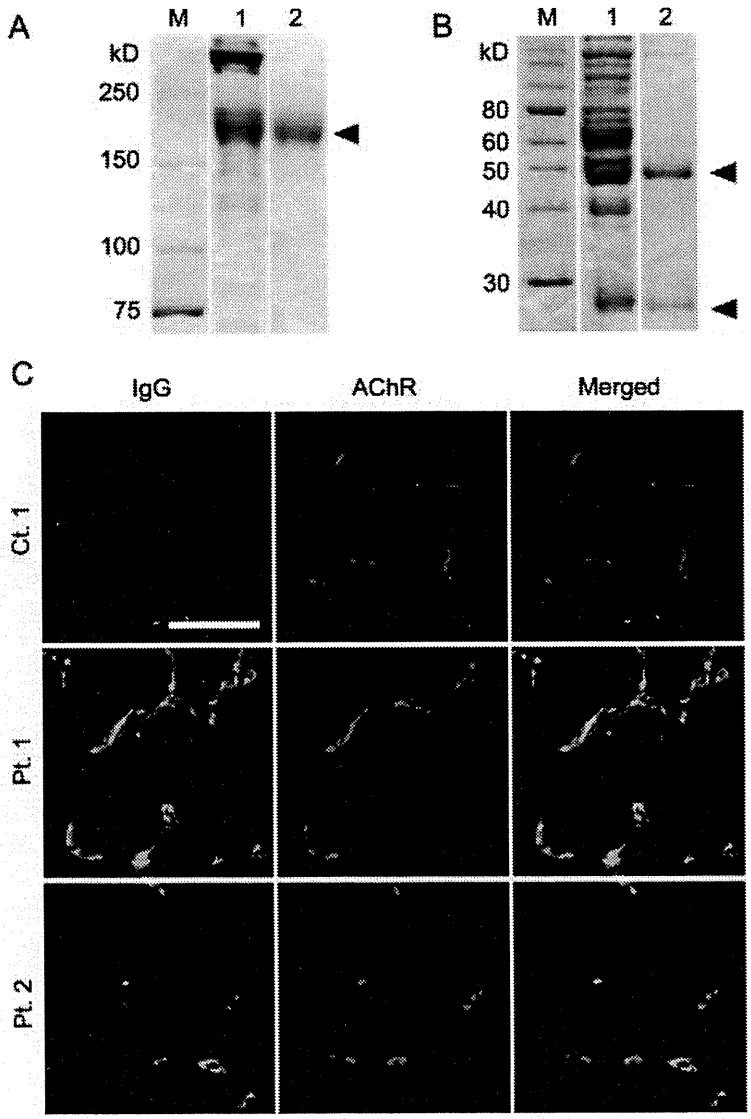

Nonreducing (A) and reducing (B) sodium dodecyl sulfate-polyacrylamide gel electrophoresis of serum proteins and purified IgG of patient 1. Gels are stained with Coomassie brilliant blue. M = molecular weight markers; 1 = serum before purification; 2 = purified IgG. Arrowheads point to IgG of 160 kD (A), as well as the heavy (50 kD) and light (25 kD) chains of IgG (B). (C) In vitro overlay of purified IgG on a 10-μm skeletal muscle section of *Colq*−/− mice. IgG is visualized with FITC-labeled antihuman IgG and acetylcholine receptor with Alexa594-labeled α-bungarotoxin. Scale bar = 50 μm.

RESULTS MuSK-IgG recognizes NMJ of a muscle section of *Colq*−/− mouse. We first confirmed that human MuSK-IgG recognizes the mouse NMJ. We isolated IgG from serum of MuSK-MG patients and confirmed the purity of IgG by Coomassie staining of nonreducing (figure 1A) and reducing (figure 1B) SDS-PAGEs. We then overlaid MuSK-IgG on quadriceps muscle sections of *Colq*−/− mice.[22] IgG of control 1 was not bound to the NMJ, whereas IgGs of patients 1 and 2 colocalized to the NMJs (figure 1C). Human MuSK-IgG thus has the potential to bind to the mouse NMJ.

In vitro overlay assay discloses that MuSK-IgG blocks binding of ColQ-tailed AChE to the NMJ of a muscle section of *Colq*−/− mouse. We previously demonstrated that the purified recombinant human ColQ-tailed AChE protein complex could bind to sections of the frog NMJs[23] and the mouse NMJs (in preparation) in vitro. Using the in vitro overlay assay, we next examined whether MuSK-IgG blocks anchoring of ColQ-tailed AChE to the mouse NMJs. We incubated a muscle section of *Colq*−/− mice with MuSK-IgG overnight at 4°C and overlaid human ColQ-tailed AChE followed by histologic visualization of ColQ and AChR (figure 2). In the presence of

Figure 2 In vitro overlay assays

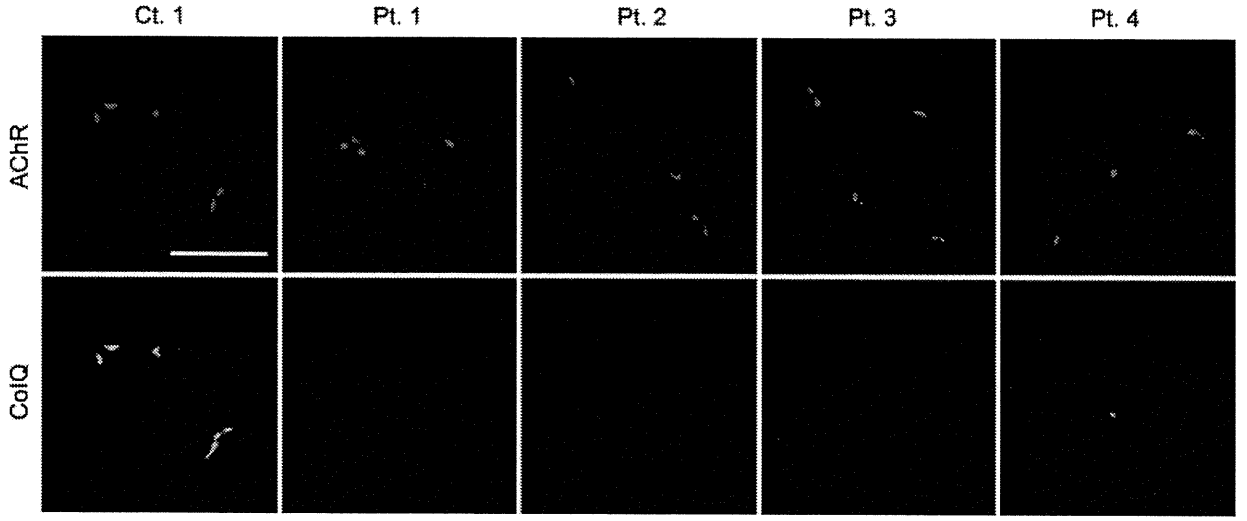

Purified recombinant collagen Q (ColQ)-tailed acetylcholinesterase (AChE) was overlaid on a 10-μm quadriceps muscle section of *Colq*−/− mice in the presence of the indicated purified muscle-specific receptor tyrosine kinase–immunoglobulin G. ColQ is stained with anti-ColQ antibody and acetylcholine receptor (AChR) with Alexa594-labeled α-bungarotoxin. Scale bar = 50 μm.

IgG of control 1, ColQ was colocalized with AChRs, whereas, in the presence of 4 MuSK-IgGs, no ColQ signal was observed at the NMJs.

In vitro plate-binding assay shows that MuSK-IgG blocks binding of ColQ-tailed AChE but not of LRP4 to MuSK. We next quantified an effect of MuSK-IgG on an interaction of human ColQ and human MuSK by an in vitro plate-binding assay. We synthesized and purified the myc-tagged extracellular domain of human MuSK (hMuSKect-myc). We then incubated an hMuSKect-coated plate with variable concentrations of control IgG or MuSK-IgG, and added a fixed amount of the purified recombinant human ColQ-tailed AChE. In 2 controls, AChE remained bound even in the presence of 100 μg of IgG, whereas in 4 MuSK-MG patients the numbers of bound AChE were proportionally decreased with increasing amounts of the patient's IgG (figure 3A).

We also examined the effect of MuSK-IgG on the interaction between the extracellular domain of MuSK and LRP4. We found that even at 100 μg IgG of control 2 or patient 2 did not block binding of LRP4 to MuSK (figure 3B).

Passive transfer model exhibits reduced ColQ signals at the NMJs. As described in the introduction, active and passive immunization of model animals reveals reduction of AChRs at the NMJs,[24,26–29] but an effect of MuSK-IgG on ColQ-tailed AChE has not been examined to date. We thus injected IgG of control 2 and patient 2 for 14 days to C57BL/6J female mice and visualized the expression of AChR, ColQ, MuSK, and AChE in quadriceps muscle sections. Signal intensities of ColQ and AChE were markedly attenuated, but the AChR and MuSK signal intensities were only moderately reduced (figure 4, A and B). Quantitative analysis of the fluorescence signals revealed that signal areas (figure 4C), intensities (figure 4D), and densities (figure 4E) of ColQ in mice injected with patient 2 IgG were significantly reduced. Conversely, signal areas (figure 4C), intensities (figure 4D), and densities (figure 4E) of AChR were only moderately reduced. Similarly, the same parameters of the MuSK signal were moderately reduced (figure 4, C, D, and E). Moderate reductions of the areas and intensities of AChR and MuSK signals are likely due to reduced sizes of the NMJs, because the densities of AChR and MuSK were only marginally affected. In addition, whereas the number of MuSK per AChR remained essentially the same, the number of ColQ per AChR was prominently reduced (figure 4F). To summarize, MuSK-IgG compromised anchoring of ColQ-tailed AChE and had a less prominent effect on the expression of MuSK and AChR.

DISCUSSION Molecular basis of MuSK-MG has been examined in cultured cells[30,31] as well as in active[28,29] and passive[24,26,27] immunization models. Application of MuSK-MG antibodies to TE671 muscle cells induces inhibition of cell proliferation and secondarily leads to downregulation of AChR and rapsyn.[30] Similarly, MuSK-MG antibodies have no or minimal effect on the cell surface expression of AChR in TE671 and C2C12 muscle cells.[31] Conversely, mice[29] and rabbits[28] immunized with recombinant MuSK develop myasthenic symptoms and

Figure 3 In vitro plate-binding assays

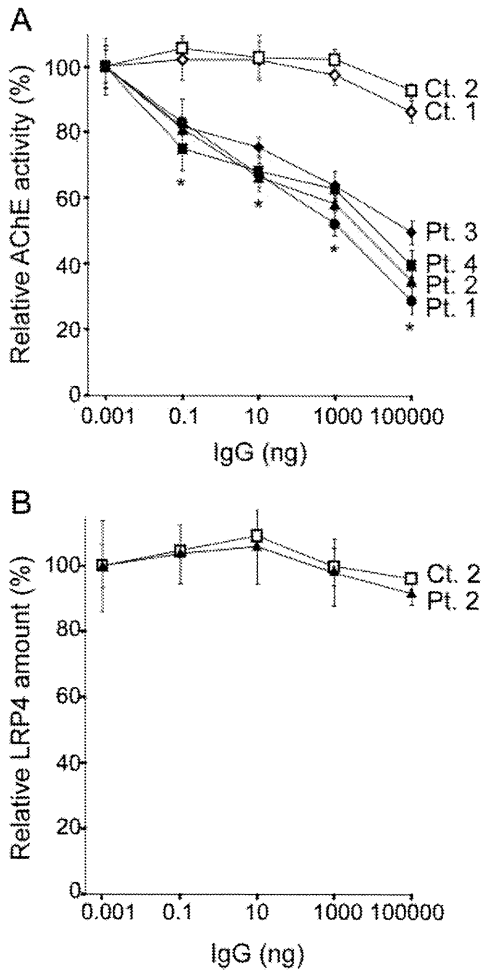

(A) Increasing amounts of muscle-specific receptor tyrosine kinase (MuSK)-immunoglobulin G (IgG) block binding of the purified recombinant collagen Q (ColQ)-tailed acetylcholinesterase (AChE) to the extracellular domain of human MuSK that is coated on a 96-well plate. Bound ColQ-tailed AChE is quantified by AChE activity. AChE activities are normalized for that at 1 pg IgG of each sample. Mean and SEM of 3 experiments are plotted. *$p < 0.01$ between controls and patients. (B) MuSK-IgG does not block binding of the purified FLAG-tagged extracellular domain of human LRP4 (LRP4N-FLAG) to MuSK that is coated on a 96-well plate. Bound LRP4N-FLAG is quantified with anti-FLAG-HRP. HRP activities are normalized for that at 1 pg IgG of each sample. Mean and SEM of 3 experiments are plotted.

NMJ AChR deficiency. Similarly, injection of MuSK-IgG into mice reduces the number of AChRs at the NMJ to 22% of controls, compromises the apposition of the presynaptic and postsynaptic components of the NMJ,[24] and reduces muscle contractility.[27] A recent report demonstrates that MuSK-IgG enhances internalization of MuSK from plasma membrane, which leads to progressive dispersal of postsynaptic AChRs by disruption of the MuSK scaffold and not by disruption of the agrin/LRP4/MuSK signaling pathway.[26] To summarize, MuSK-IgG does not reduce AChR expression in cultured cells, but active and passive immunization of model animals results in AChR deficiency, which is not likely due to blocking of the agrin/LRP4/MuSK pathway. Our findings that MuSK-IgG blocks binding of ColQ but not of LRP4 to MuSK are consistent with these findings. In myotubes of *Colq*−/− mice, the number of membrane-bound MuSK is prominently reduced, and agrin-mediated phosphorylation of the AChR β subunit and the subsequent clustering of AChR are reduced to 30%–50% of the wild type.[32] Thus, compromised clustering of AChRs at the NMJs in some MuSK-MG patients could result from blocking of ColQ binding to MuSK but not from blocking of LRP4 binding to MuSK.

Although our results predict endplate AChE deficiency in MuSK-MG patients, we found no AChE deficiency in intercostal muscles of one reported[33] and two unreported cases of MuSK-MG. In vitro microelectrode studies showed a normal EPP decay time constant.[34] In the 3 MuSK-MG patients observed by us, the MEPC decay times were shorter than normal, normal, and 2-fold prolonged[33] compared to controls. Thus, our biopsy findings do not indicate that MuSK-MG patients have endplate AChE deficiency. There are 2 plausible explanations for the apparently contradicting observation on the human biopsies and the in vitro and in vivo studies. First, MuSK-IgG does not block binding of ColQ-tailed AChE to the NMJ to a detectable extent in the patients. ColQ is localized to the synaptic basal lamina via 2 mechanisms: one is by binding to heparin sulfate proteoglycans including perlecan,[7,8] and the other is by binding to MuSK.[9] We previously reported that both mechanisms are required for in vitro anchoring of human ColQ to the frog NMJ.[23] Reduced clustering of ColQ in our passive transfer model suggests that ColQ needs to bind to at least MuSK in mice. However, binding of ColQ to MuSK is dispensable for clustering ColQ in humans, but is required for facilitating AChR clustering.[32] Second, AChE could be deficient in severely affected muscles but not in the biopsied intercostal muscles. However, the respiratory functions of the patients who had intercostal muscle biopsies were severely compromised. Expression levels of MuSK[35] and ColQ[36] were reported to be different between slow- and fast-twitch muscles in model animals. In active[37] and passive[26] immunization models, slow-twitch diaphragm was more severely affected than fast-twitch tibialis anterior and intercostal muscles. Similar uneven distributions of affected muscles are reported in MuSK-MG patients.[12] Further studies will be required to elucidate the basis of the discrepant observations between mice and humans.

Figure 4 **Passive transfer of muscle-specific receptor tyrosine kinase (MuSK)–immunoglobulin G (IgG) of control 2 and patient 2 to C57BL/6J mice**

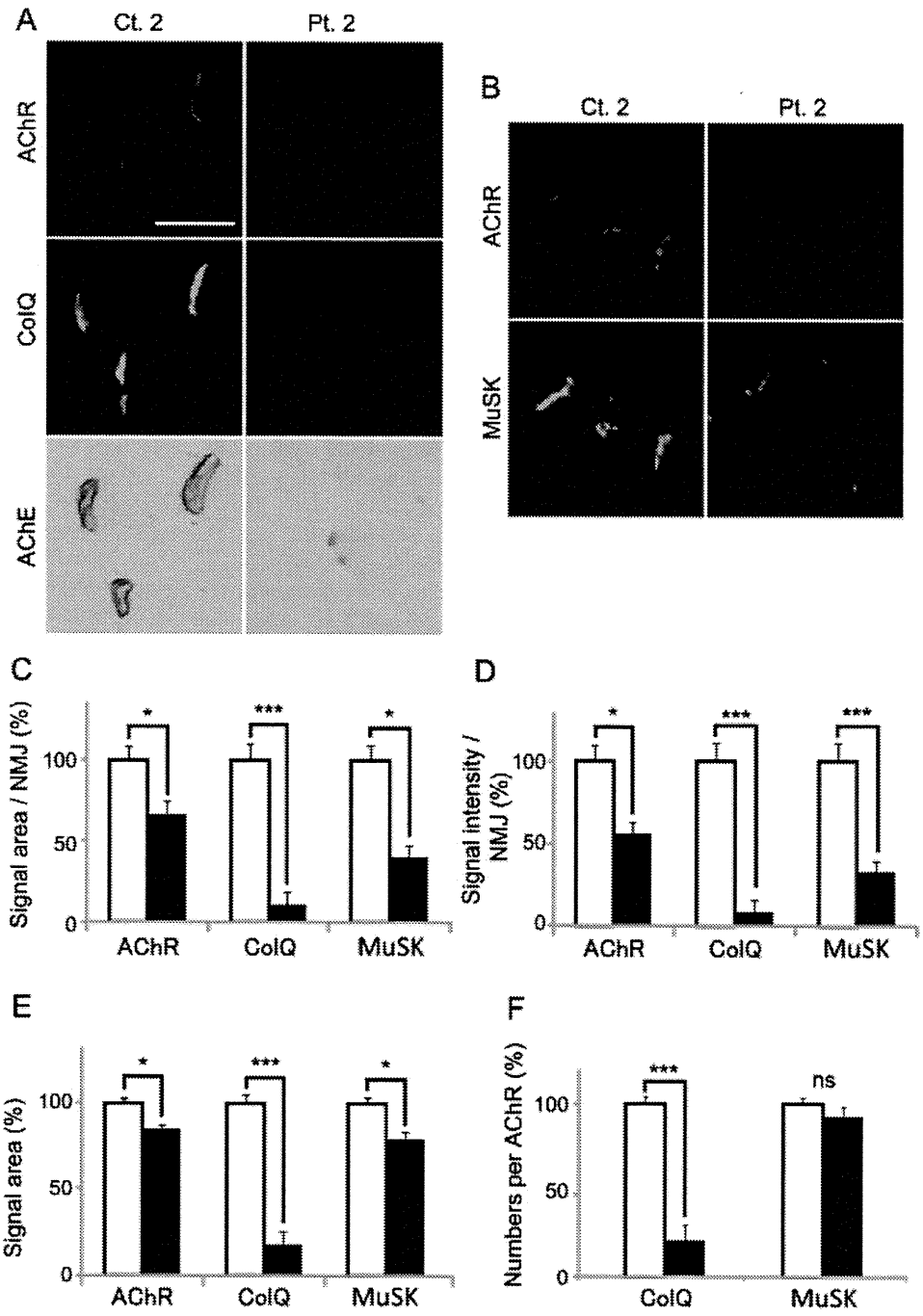

(A, B) Quadriceps muscle sections of mice injected with IgG of control 2 or patient 2 are stained for acetylcholine receptor (AChR) by Alexa594-labeled α-bungarotoxin, collagen Q (ColQ) and MuSK by immunostaining, acetylcholinesterase (AChE) by cytochemical staining. Scale bar = 40 μm. Signal areas (C), intensities (D), and densities (intensity/area) (E) of the indicted molecules per neuromuscular junction (NMJ) are shown in mean and SEM. (F) Densities of ColQ and MuSK are normalized for the density of AChR to estimate the number of ColQ and MuSK per AChR. For AChR, ColQ, and MuSK, we analyzed 44 NMJs of control 2 and 23 NMJs of patient 2. For MuSK, we analyzed 82 NMJs of control 2 and 42 NMJs of patient 2. Areas and intensities are quantified by the BZ-9000 microscope (Keyence). Open and closed bars represent control 2 and patient 2, respectively. $^{*}p < 0.05$, $^{***}p < 0.001$. NS = not significant.

AUTHOR CONTRIBUTIONS

Dr. Kawakami designed and conducted experiments and wrote the paper. Dr. Ito designed and conducted experiments. Dr. Hirayama conducted experiments. Dr. Sahashi diagnosed a patient and conceived the study. Dr. Ohkawara designed experiments. Dr. Masuda designed experiments. Dr. Nishida diagnosed a patient and conceived the study. Dr. Mabuchi diagnosed a patient and conceived the study. Dr. Engel diagnosed a patient, conceived studies, designed experiments, and wrote the paper. Dr. Ohno conceived study, designed experiments, and wrote the paper.

ACKNOWLEDGMENT

The authors thank Kenji Otsuka for technical assistance and the patients who participated in this study.

DISCLOSURE

Dr. Kawakami, Dr. Ito, Dr. Hirayama, Dr. Sahashi, Dr. Ohkawara, Dr. Masuda, Dr. Nishida, and Dr. Mabuchi report no disclosures. Dr. Engel serves as an Associate Editor of *Neurology*®; receives publishing royalties for *Myology 3rd ed.* (McGraw-Hill, 2004); and has received research support from the NIH and the Muscular Dystrophy Association. Dr. Ohno has received Grants-in-Aids from the Japan Society for the Promotion of Science, the Ministry of Health, Labour and Welfare, and the Japan Science and Technology Agency.

Received March 21, 2011. Accepted in final form May 12, 2011.

REFERENCES

1. Kim N, Stiegler AL, Cameron TO, et al. Lrp4 is a receptor for Agrin and forms a complex with MuSK. Cell 2008; 135:334–342.
2. Zhang B, Luo S, Wang Q, Suzuki T, Xiong WC, Mei L. LRP4 serves as a coreceptor of agrin. Neuron 2008;60: 285–297.
3. Dechiara TM, Bowen DC, Valenzuela DM, et al. The receptor tyrosine kinase MuSK is required for neuromuscular junction formation in vivo. Cell 1996;85:501–512.
4. Okada K, Inoue A, Okada M, et al. The muscle protein Dok-7 is essential for neuromuscular synaptogenesis. Science 2006;312:1802–1805.
5. Wu H, Xiong WC, Mei L. To build a synapse: signaling pathways in neuromuscular junction assembly. Development 2010;137:1017–1033.
6. Krejci E, Thomine S, Boschetti N, Legay C, Sketelj J, Massoulié J. The mammalian gene of acetylcholinesterase-associated collagen. J Biol Chem 1997;272:22840–22847.
7. Deprez P, Inestrosa NC, Krejci E. Two different heparin-binding domains in the triple-helical domain of ColQ, the collagen tail subunit of synaptic acetylcholinesterase. J Biol Chem 2003;278:23233–23242.
8. Peng HB, Xie H, Rossi SG, Rotundo RL. Acetylcholinesterase clustering at the neuromuscular junction involves perlecan and dystroglycan. J Cell Biol 1999;145:911–921.
9. Cartaud A, Strochlic L, Guerra M, et al. MuSK is required for anchoring acetylcholinesterase at the neuromuscular junction. J Cell Biol 2004;165:505–515.
10. Farrugia ME, Vincent A. Autoimmune mediated neuromuscular junction defects. Curr Opin Neurol 2010;23: 489–495.
11. Farrugia ME, Robson MD, Clover L, et al. MRI and clinical studies of facial and bulbar muscle involvement in MuSK antibody-associated myasthenia gravis. Brain 2006; 129:1481–1492.
12. Evoli A, Tonali PA, Padua L, et al. Clinical correlates with anti-MuSK antibodies in generalized seronegative myasthenia gravis. Brain 2003;126:2304–2311.
13. Sanders DB, El-Salem K, Massey JM, McConville J, Vincent A. Clinical aspects of MuSK antibody positive seronegative MG. Neurology 2003;60:1978–1980.
14. Hatanaka Y, Hemmi S, Morgan MB, et al. Nonresponsiveness to anticholinesterase agents in patients with MuSK-antibody-positive MG. Neurology 2005;65:1508–1509.
15. Pasnoor M, Wolfe GI, Nations S, et al. Clinical findings in MuSK-antibody positive myasthenia gravis: a U.S. experience. Muscle Nerve 2010;41:370–374.
16. McConville J, Farrugia ME, Beeson D, et al. Detection and characterization of MuSK antibodies in seronegative myasthenia gravis. Ann Neurol 2004;55:580–584.
17. Shiraishi H, Motomura M, Yoshimura T, et al. Acetylcholine receptors loss and postsynaptic damage in MuSK antibody-positive myasthenia gravis. Ann Neurol 2005;57: 289–293.
18. Niks EH, van Leeuwen Y, Leite MI, et al. Clinical fluctuations in MuSK myasthenia gravis are related to antigen-specific IgG4 instead of IgG1. J Neuroimmunol 2008; 195:151–156.
19. Ohno K, Brengman J, Tsujino A, Engel AG. Human endplate acetylcholinesterase deficiency caused by mutations in the collagen-like tail subunit (ColQ) of the asymmetric enzyme. Proc Natl Acad Sci USA 1998;95:9654–9659.
20. Okada T, Shimazaki K, Nomoto T, et al. Adeno-associated viral vector-mediated gene therapy of ischemia-induced neuronal death. Methods Enzymol 2002;346: 378–393.
21. Horejsi J, Smetana R. The isolation of gamma globulin from blood-serum by rivanol. Acta Med Scand 1956;155: 65–70.
22. Feng G, Krejci E, Molgo J, Cunningham JM, Massoulie J, Sanes JR. Genetic analysis of collagen Q: roles in acetylcholinesterase and butyrylcholinesterase assembly and in synaptic structure and function. J Cell Biol 1999;144: 1349–1360.
23. Kimbell LM, Ohno K, Engel AG, Rotundo RL. C-terminal and heparin-binding domains of collagenic tail subunit are both essential for anchoring acetylcholinesterase at the synapse. J Biol Chem 2004;279:10997–11005.
24. Cole RN, Reddel SW, Gervasio OL, Phillips WD. Anti-MuSK patient antibodies disrupt the mouse neuromuscular junction. Ann Neurol 2008;63:782–789.
25. Toyka KV, Drachman DB, Griffin DE, et al. Myasthenia gravis: study of humoral immune mechanisms by passive transfer to mice. N Engl J Med 1977;296:125–131.
26. Cole RN, Ghazanfari N, Ngo ST, Gervasio OL, Reddel SW, Phillips WD. Patient autoantibodies deplete postsynaptic muscle-specific kinase leading to disassembly of the ACh receptor scaffold and myasthenia gravis in mice. J Physiol 2010;588:3217–3229.
27. ter Beek WP, Martinez-Martinez P, Losen M, et al. The effect of plasma from muscle-specific tyrosine kinase myasthenia patients on regenerating endplates. Am J Pathol 2009;175:1536–1544.
28. Shigemoto K, Kubo S, Maruyama N, et al. Induction of myasthenia by immunization against muscle-specific kinase. J Clin Invest 2006;116:1016–1024.
29. Jha S, Xu K, Maruta T, et al. Myasthenia gravis induced in mice by immunization with the recombinant extracellular domain of rat muscle-specific kinase (MuSK). J Neuroimmunol 2006;175:107–117.
30. Boneva N, Frenkian-Cuvelier M, Bidault J, Brenner T, Berrih-Aknin S. Major pathogenic effects of anti-MuSK antibodies in myasthenia gravis. J Neuroimmunol 2006; 177:119–131.
31. Farrugia ME, Bonifati DM, Clover L, Cossins J, Beeson D, Vincent A. Effect of sera from AChR-antibody negative myasthenia gravis patients on AChR and MuSK in cell cultures. J Neuroimmunol 2007;185:136–144.
32. Sigoillot SM, Bourgeois F, Lambergeon M, Strochlic L, Legay C. ColQ controls postsynaptic differentiation at the neuromuscular junction. J Neurosci 2010;30:13–23.

33. Selcen D, Fukuda T, Shen X-M, Engel AG. Are MuSK antibodies the primary cause of myasthenic symptoms? Neurology 2004;62:1945–1950.
34. Niks EH, Kuks JB, Wokke JH, et al. Pre- and postsynaptic neuromuscular junction abnormalities in musk myasthenia. Muscle Nerve 2010;42:283.
35. Punga AR, Maj M, Lin S, Meinen S, Ruegg MA. MuSK levels differ between adult skeletal muscles and influence postsynaptic plasticity. Eur J Neurosci 2011;33:890–898.
36. Krejci E, Legay C, Thomine S, Sketelj J, Massoulie J. Differences in expression of acetylcholinesterase and collagen Q control the distribution and oligomerization of the collagen-tailed forms in fast and slow muscles. J Neurosci 1999;19:10672–10679.
37. Xu K, Jha S, Hoch W, Dryer SE. Delayed synapsing muscles are more severely affected in an experimental model of MuSK-induced myasthenia gravis. Neuroscience 2006; 143:655–659.

Call for Submissions: *Neurology* launches Global Perspectives!

In October 2011, *Neurology*® will launch Global Perspectives, an expanded and enhanced version of the International Newsletter. New Co-Editors Johan A. Aarli, MD, and Oded Abramsky, MD, PhD, FRCP, encourage submissions to this section that will provide a platform in *Neurology* for publishing news about scientific findings or academic issues. News may include international research content, spotlights on specific neurologic practice concerns within a country, or important information about international educational or scientific collaborative efforts.

Submissions must be 1,250 words or less with five or less references. A maximum of two figures or two tables (or combination) can be incorporated if necessary. For complete submission requirements, please go to *www.neurology.org* and click on "Information for Authors." The submissions will be reviewed by the editors and may be edited for clarity.

Interested submitters can register and upload manuscripts under the section "Global Perspectives" at *http://submit.neurology.org*. Please send inquiries to Kathy Pieper, Managing Editor, *Neurology; kpieper@neurology.org*.

Neurology® Launches WriteClick Join the Debate!

Neurology.org has launched WriteClick and the editors encourage comments about recent articles.

Go to *www.neurology.org* and click on the "WriteClick" tab at the top of the page. Responses will be posted within 72 hours of submission.

Before using WriteClick, remember the following:

- WriteClick is restricted to comments about studies published in *Neurology* within the last eight weeks
- Read previously posted comments; redundant comments will not be posted
- Your submission must be 200 words or less and have a maximum of five references; reference one must be the article on which you are commenting
- You can include a maximum of five authors (including yourself)

SCIENTIFIC REPORTS

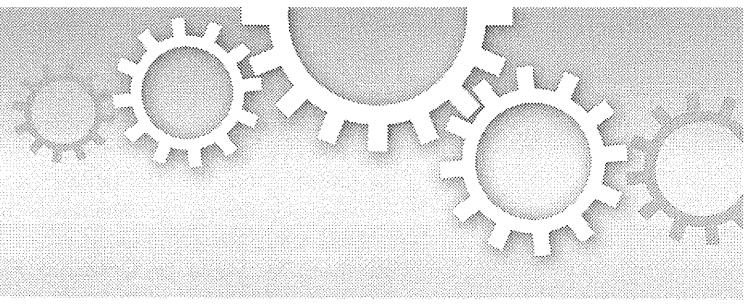

CUGBP1 and MBNL1 preferentially bind to 3′ UTRs and facilitate mRNA decay

Akio Masuda[1], Henriette Skovgaard Andersen[2]*, Thomas Koed Doktor[2]*, Takaaki Okamoto[1], Mikako Ito[1], Brage Storstein Andresen[2] & Kinji Ohno[1]

[1]Division of Neurogenetics, Center for Neurological Diseases and Cancer, Nagoya University Graduate School of Medicine, Nagoya, Japan, [2]Department of Biochemistry and Molecular Biology, University of Southern Denmark, Odense M, Denmark.

SUBJECT AREAS:
CELLULAR NEUROSCIENCE
MOTOR SYSTEM
GENE REGULATION
TRANSCRIPTOME

Received
25 August 2011

Accepted
8 December 2011

Published
4 January 2012

Correspondence and requests for materials should be addressed to K.O. (ohnok@med.nagoya-u.ac.jp)

* These authors contributed equally to this work.

CUGBP1 and MBNL1 are developmentally regulated RNA-binding proteins that are causally associated with myotonic dystrophy type 1. We globally determined the *in vivo* RNA-binding sites of CUGBP1 and MBNL1. Interestingly, CUGBP1 and MBNL1 are both preferentially bound to 3′ UTRs. Analysis of CUGBP1- and MBNL1-bound 3′ UTRs demonstrated that both factors mediate accelerated mRNA decay and temporal profiles of expression arrays supported this. Role of CUGBP1 on accelerated mRNA decay has been previously reported, but the similar function of MBNL1 has not been reported to date. It is well established that CUGBP1 and MBNL1 regulate alternative splicing. Screening by exon array and validation by RT-PCR revealed position dependence of CUGBP1- and MBNL1-binding sites on the resulting alternative splicing pattern. This study suggests that regulation of CUGBP1 and MBNL1 is essential for accurate control of destabilization of a broad spectrum of mRNAs as well as of alternative splicing events.

In recent years, new technologies, such as microarray analysis and high throughput sequencing, have dramatically changed our knowledge on gene expression and revealed that extensive regulation takes place during posttranscriptional RNA processing[1]. Numerous RNA processing elements and regulatory RNA-binding proteins play together in a finely tuned interplay to ensure that different mRNAs are made from the primary transcript from a gene and are present in the right cell at the right time and in the correct amounts. Such complex regulation is of course vulnerable and a rapidly increasing number of human diseases are now known to be caused by misregulated RNA processing[2]. An intriguing example where this kind of disease mechanism is in operation is myotonic dystrophy type 1 (DM1), where aberrant regulation of two RNA-binding proteins, CUG-binding protein 1 (CUGBP1) and muscleblind-like 1 (MBNL1) co-operationally cause some of the disease symptoms. DM1 is the most common form of myotonic dystrophy (DM), and is caused by an expansion of CTG-repeats in the 3′ untranslated region (UTR) of the DM protein kinase gene (*DMPK*) on chromosome 19[3–5]. DM1 is a multisystemic disorder and the clinical features include myotonia, muscle degeneration, heart failure, ocular cataracts, impaired glucose tolerance, and mental retardation[6,7]. A dominant negative effect of the *DMPK* mutant allele through RNA gain-of-function has been proposed as the molecular disease mechanism. Many studies support a mechanism where toxic *DMPK* RNA with expanded CUG repeats binds to and sequesters proteins that are important for RNA metabolism including transcription, RNA transport, alternative splicing, translation, and yet unknown processes[6]. The expanded CUG repeats in the *DMPK* mRNA bind to and sequestrate MBNL1 in discrete nuclear foci, which results in depletion of functional MBNL1[8,9]. By a yet unknown mechanism the expanded CUG repeats also activate protein kinase C (PKC), which phosphorylates and stabilizes CUGBP1[10]. Thus, the expanded CUG repeats contribute to DM1 pathogenesis by causing loss of MBNL1 and gain of CUGBP1 activity[11].

Both CUGBP1 and MBNL1 regulate postnatal transitions in alternative splicing patterns during striated muscle development[9,12,13]. Representative targets of CUGBP1 splicing regulation, which are misregulated in DM1 striated muscles, include genes for cardiac troponin T (*TNNT2*)[14,15], insulin receptor (*INSR*)[16], and chloride channel 1 (*CLCN1*)[15,17]. MBNL1 contains four CCCH-type zinc fingers that recognize a YGCY motif that is indeed observed in the CUG repeat (CUGCUG)[18–21]. Mice deficient in *Mbnl1* show aberrant splicing of *Clcn1*, *Tnnt2*, and *Tnnt3*, but not *Insr*[22]. Very recently, MBNL1 was shown to regulate *BIN1* alternative splicing, and dysregulation of *BIN1* splicing in DM1 muscles was suggested to be part of the disease pathology resulting in muscle weakness[23]. Besides an important role in splicing regulation, CUGBP1 mediates mRNA decay of short-lived transcripts by interaction with GU-rich elements in the 3′ UTR[24–27]. In addition, CUGBP1 increases the translation of *CDKN1A*[28] and *Mef2a*[29]. In contrast to the multiple functionalities in posttranscriptional gene regulation of CUGBP1, MBNL1 has so far been exclusively recognized as a splicing regulatory *trans*-factor.

High-throughput sequencing of RNA isolated by crosslinking immunoprecipitation (HITS-CLIP)[30] is a new method that enables global mapping of targets for specific RNA-binding proteins in living cells, thereby shedding light on their role in regulation of RNA processing of known and unknown targets.

In the present study, we performed HITS-CLIP analysis for CUGBP1 and MBNL1 on the mouse myoblast cell line C2C12 to extensively characterize their RNA-binding sites and functional roles in RNA processing. We identified position-dependence of CUGBP1/MBNL1-binding sites in regulating exon inclusion or skipping. Interestingly, we discovered that both CUGBP1 and MBNL1 preferentially bind to the 3′ UTR and destabilize target mRNAs. This points to a new important role of MBNL1 and suggests that binding to the 3′ UTRs and destabilization of mRNA are likely to be a fundamental function shared by CUGBP1 and MBNL1.

Results

Genome-wide CUGBP1/MBNL1-RNA interaction maps. In order to determine global CUGBP1/MBNL1-binding sites *in vivo*, we performed HITS-CLIP experiments using the mouse myoblast cell line, C2C12.

In C2C12 cells, CUGBP1 is constantly expressed throughout myoblast differentiation, whereas expression of MBNL1 is low in undifferentiated cells and gradually increases during differentiation (Supplementary Fig. S1), as previously described[8]. We thus performed HITS-CLIP analysis of CUGBP1 and MBNL1 using undifferentiated and differentiated C2C12 cells, respectively. We also performed CLIP of MBNL1 using undifferentiated cells in three independent experiments, but this yielded an insufficient amount of RNA-protein complexes and failed to yield cDNA libraries suitable for high-throughput sequencing. In the HITS-CLIP analysis of CUGBP1, our first experiment yielded 34,733,815 CLIP tags of 32 nt, of which 29,545,067 (85.06%) were mapped to the mm9 genome allowing at most 2 mismatches and placing reads mapping to multiple locations to a single random site. A second CLIP experiment yielded 10,079,185 CLIP tags of 36 nt, of which 8,516,256 (84.49%) were mapped. In the first MBNL1 CLIP experiment, we obtained 13,218,685 CLIP tags, of which 11,044,152 (83.55%) were mapped, while the second CLIP experiment yielded 13,474,600 CLIP tags with 11,455,886 (85.02%) tags mapped to the mm9 genome. For the analysis of binding motif and binding region annotation, we selected only reads that were aligned uniquely in the genome and removed all potential PCR duplicates by collapsing reads with an identical 5′ start into a single read. This resulted in 177,013 and 130,828 CLIP tags from the two CUGBP1 CLIP experiments, while the two MBNL1 experiments yielded 59,156 and 583,841 CLIP tags respectively.

In an effort to confirm the specificity of our CLIP experiments, we performed CLIP analysis of polypyrimidine tract-binding protein (PTB), a multifunctional RNA-binding protein, using undifferentiated mouse C2C12 cells. We identified 12,841,778 CLIP tags of which 11,184,829 (87.10%) were mapped to the mouse mm9 genome. Removal of non-uniquely aligned reads and PCR duplicates yielded 307,995 unambiguous CLIP tags.

Consensus motifs. To determine RNA-binding motifs associated with CUGBP1/MBNL1 *in vivo*, we used the motif-finding algorithm, Multiple EM for Motif Elicitation (MEME)[31]. We used SeqMonk to identify likely binding regions, and identified 1,841 CUGBP1-binding regions and 302 MBNL1-binding regions. Comparison of SeqMonk's maximum depth scores between samples indicates that binding regions in each replicated experiment are highly overlapping, while PTB binding regions did not overlap with those of the other four CLIP experiments (Supplementary Fig. S2). The lower number of identified MBNL1 regions supported by two independent experiments (Supplementary Fig. S2b) was likely due to the large difference in the number of CLIP tags in the two MBNL1 experiments. The regions demonstrate enrichment of GU-rich motifs for CUGBP1 and YGCY-containing motifs for MBNL1 (Fig. 1).

Our *in vivo* binding motifs are in accordance with previously suggested binding motifs for CUGBP1[25,32] and MBNL1[21,33–35]. We identified 1,824 PTB binding regions in the mouse genome and detected a CU-rich motif, which is essentially identical to the motif for PTB recently identified by HITS-CLIP analysis of a human cell line[36].

We also analyzed the CUGBP1 and MBNL1 motifs enriched in regions containing reads with multiple potential mapping locations (Supplementary Fig. S3), and compared them with the motifs with unique mapping (Fig. 1). Following removal of potential PCR duplicates, we observed 699,382 tags that were non-uniquely aligned in the 1st CUGBP1 CLIP experiment, 219,128 tags in the 2nd CUGBP1 CLIP experiment, 105,432 and 216,882 tags in the two MBNL1 CLIP experiments respectively and finally 851,324 tags in the PTB CLIP experiment. We observed that enriched motifs in these regions (Supplementary Fig. S3) are very similar to the CUGBP1 and MBNL1 motifs enriched in the binding regions containing uniquely aligned reads (Fig. 1), suggesting that these regions share the same properties as the uniquely aligned regions and that they may contain functional binding sites.

HITS-CLIP analysis of splicing targets. We next studied the effects of CUGBP1/MBNL1 binding on alternative splicing. CUGBP1 tags are clustered in intronic regions flanking alternative rather than

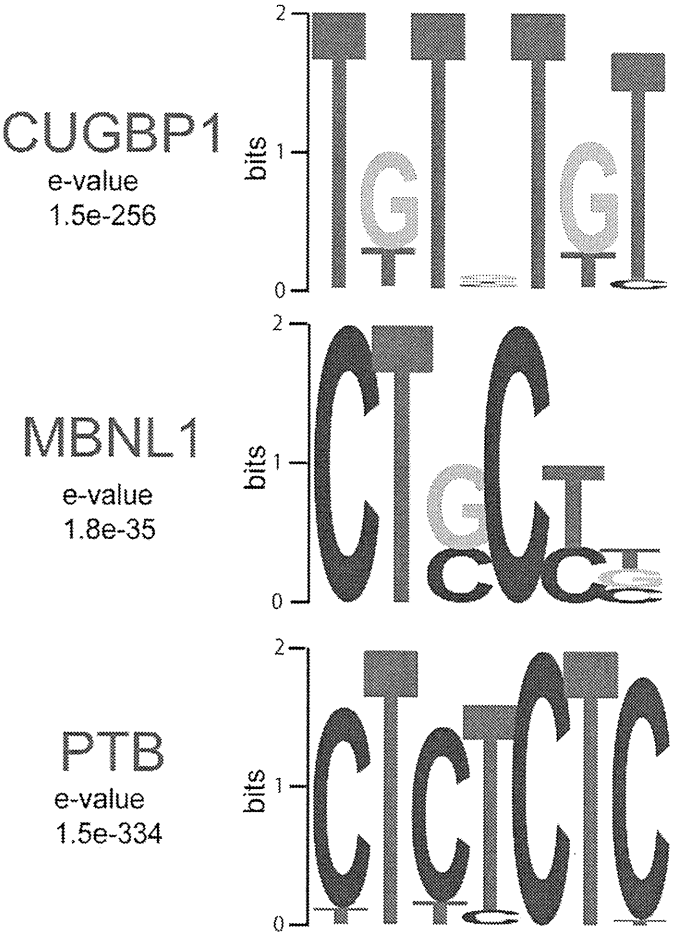

Figure 1 | Binding motif analysis. WebLogos of consensus binding motifs of CUGBP1, MBNL1, and PTB generated by the MEME motif analysis tool. The likelihood of finding the indicated motif by chance is indicated as an E-value.

constitutive exons (Fig. 2a). MBNL1 tags are similarly clustered in intronic regions flanking alternative exons, and are also enriched in alternative and constitutive exons. In order to investigate if and how CUGBP1/MBNL1 binding around splice sites regulate alternative splicing, we knocked down these factors by siRNA in undifferentiated C2C12 cells (Supplementary Fig. S4a). We analyzed alterations of splicing globally using the Affymetrix Mouse Exon 1.0 ST Array (GEO accession number, GSE29990) and identified 8 CUGBP1-responsive and 24 MBNL1-responsive exons (Supplementary Table 1, Figs. S5 and S6abc). We also analyzed 29 CUGBP1-tagged and 51 MBNL1-tagged exons/introns known to be alternatively spliced according to the ENSEMBL version *e!*61, and identified 16 CUGBP1-responsive and 21 MBNL1-responsive exons by RT-PCR (Supplementary Figs. S5 and S6abc). We made the compiled dataset C, which is comprised of the 24 CUGBP1-regulated exons (15 skipped and 9 included), as well as the compiled dataset M consisting of the 45 MBNL1-regulated exons (25 skipped and 20 included). The datasets include 1 and 9 previously identified target exons of CUGBP1 and MBNL1, respectively (Supplementary Fig. S5). In addition, 9 exons are shared between datasets C and M. Mbnl1 siRNA sufficiently suppressed MBNL1 expression up to day 3 after differentiation (Supplementary Fig. S4b), and we observed that as many as 44 of the 45 MBNL1-regulated exons in dataset M respond similarly to MBNL1 knockdown in both differentiated and undifferentiated cells (Supplementary Figs. S4 and S5).

We also made dataset M2 that includes 26 additional MBNL1-dependent cassette exons (15 skipped and 11 included) that were previously identified in skeletal muscle of MBNL1 knockout mice

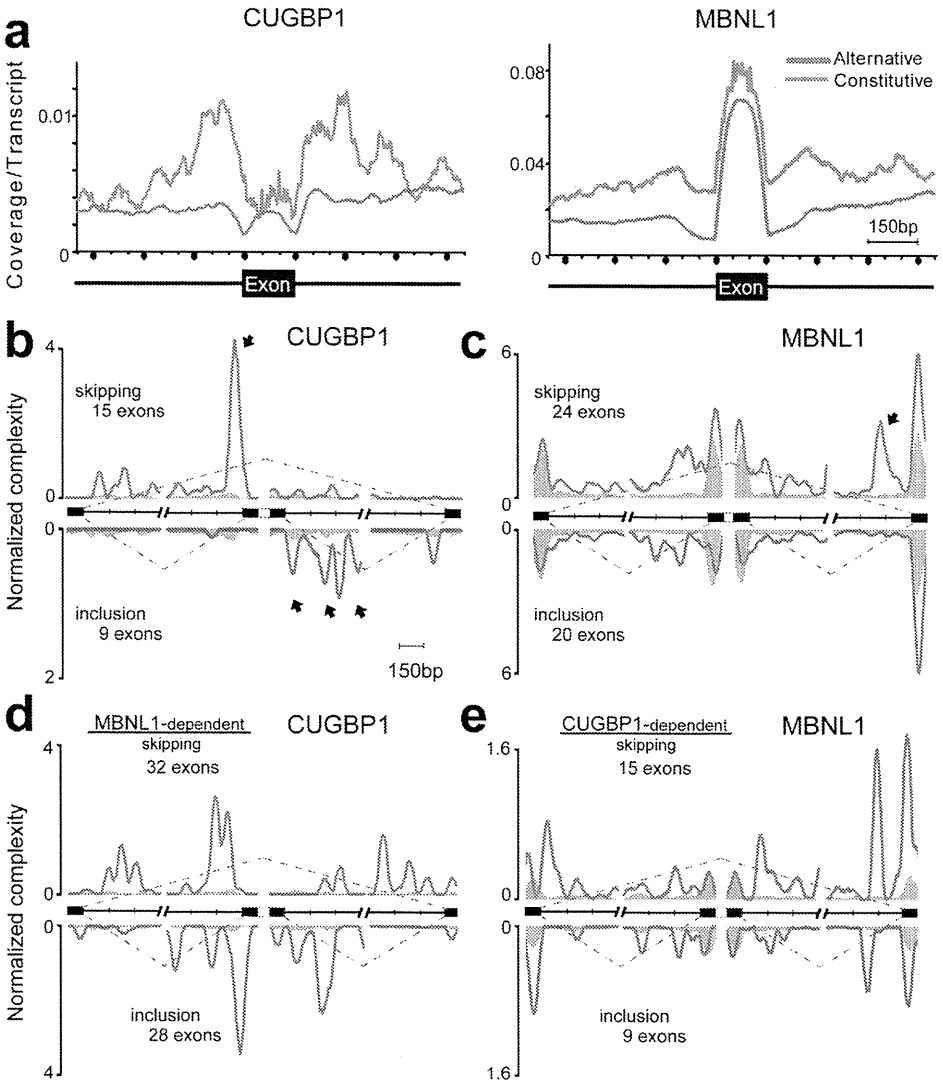

Figure 2 | Mapping of CLIP-tags on exon-intron structures. (a) Distributions of CLIP-tags on constitutively or alternatively spliced exons and the flanking intronic regions. The abscissa indicates an intron-exon-intron structure. The sizes of all the exons are normalized to 150 nucleotides. Numbers of exonic CLIP-tags are also normalized accordingly. Intronic CLIP-tags within 500 nucleotides upstream or downstream of exons are indicated. The number of CLIP-tags is normalized for the number of transcripts belonging to either category of constitutive and alternative exons. (b) Normalized complexity map of CUGBP1 at CUGBP1-dependent splice sites. Twenty-four CUGBP1-regulated splicing events in dataset C in undifferentiated C2C12 cells are compiled. (c) Normalized complexity map of MBNL1 at MBNL1-dependent splice sites. Forty-four MBNL1-regulated splicing events in differentiated C2C12 cells in dataset M are compiled. (d) Normalized complexity map of CUGBP1 at MBNL1-dependent splice sites. Sixty MBNL1-regulated splicing events in undifferentiated C2C12 cells in datasets M and M2 are compiled. (e) Normalized complexity map of MBNL1 at CUGBP1-dependent splice sites. Twenty-four CUGBP1-regulated splicing events in undifferentiated C2C12 cells in dataset C are compiled. Shaded areas represent an average of 100 sets of normalized complexity of 50 (b, c, and d) and 15 (e) randomly selected constitutive exons. Arrows indicate representative peaks that are explained in Results. Graphs represents results of the 2nd CLIP experiments for both CUGBP1 and MBNL1. Resutls of the 1st CLIP experiments are shown in Supplmentary Fig. S7.

(Supplementary Table S2)[33], and found that 18 exons are similarly regulated by *Mbnl1* knockdown in undifferentiated C2C12 cells (Supplementary Fig. S6d and Table S2).

We combined datasets C and M into a single composite pre-mRNA and made integrated RNA maps from our HITS-CLIP reads mapped to the corresponding genomic regions as previously described for Nova[30] and PTB[36]. This showed that CUGBP1 binding to upstream intronic regions facilitates exon skipping, whereas CUGBP1 binding to downstream intronic regions promotes exon inclusion (closed arrows in Fig. 2b and Supplementary Fig. S7a). Results of the 2nd experiments are shown in Fig. 2 and those of the 1st experiments are in Supplementary Fig. S7. In contrast, although the binding sites of MBNL1 are more diffusely distributed and less abundant in regions flanking splice sites (Fig. 2c), MBNL1 binding close to the 3′ end of the downstream intron induces exon skipping (closed arrow in Fig. 2c and Supplementary Fig. S7b). The presence of a similar peak in dataset M2 (closed arrow in Supplementary Fig. S7c) further supports this observation.

We next analyzed the interaction between CUGBP1 and MBNL1 in splicing regulation. We made an RNA map of CUGBP1-binding sites in MBNL1-regulated exons from datasets M and M2 (Fig. 2d and Supplementary Fig. S7e), as well as an RNA map of MBNL1-binding sites in CUGBP1-regulated exons from dataset C (Fig. 2e and Supplementary Fig. S7f). Both RNA maps demonstrate the presence of CUGBP1 clusters in MBNL1-responsive exons and vice versa, which suggests that CUGBP1 and MBNL1 are likely to regulate alternative splicing of some of the same exons.

MBNL1 and CUGBP1 both preferentially bind to the 3′ UTR. MBNL1 has so far solely been categorized as an exon/intron-binding splicing regulatory protein[6], but to our surprise we found that the majority (55%) of MBNL1-binding regions are located in 3′ UTRs (Fig. 3a). The same pattern with preferential binding (53%) in 3′ UTRs is observed for CUGBP1, while only 2% of PTB binding regions are located in 3′ UTRs (Fig. 3a). Similarly, when HITS-CLIP tags are mapped to the size-normalized positions of all the genes in the mouse genome, CUGBP1 and MBNL1 CLIP tags, but not PTB CLIP-tags, are enriched close to the 3′ ends of genes (Fig. 3b). Additionally, 610 3′ UTRs, which constitutes 28.7% of the CUGBP1-tagged 3′ UTRs and 17.4% of the MBNL1-tagged 3′ UTRs, are shared

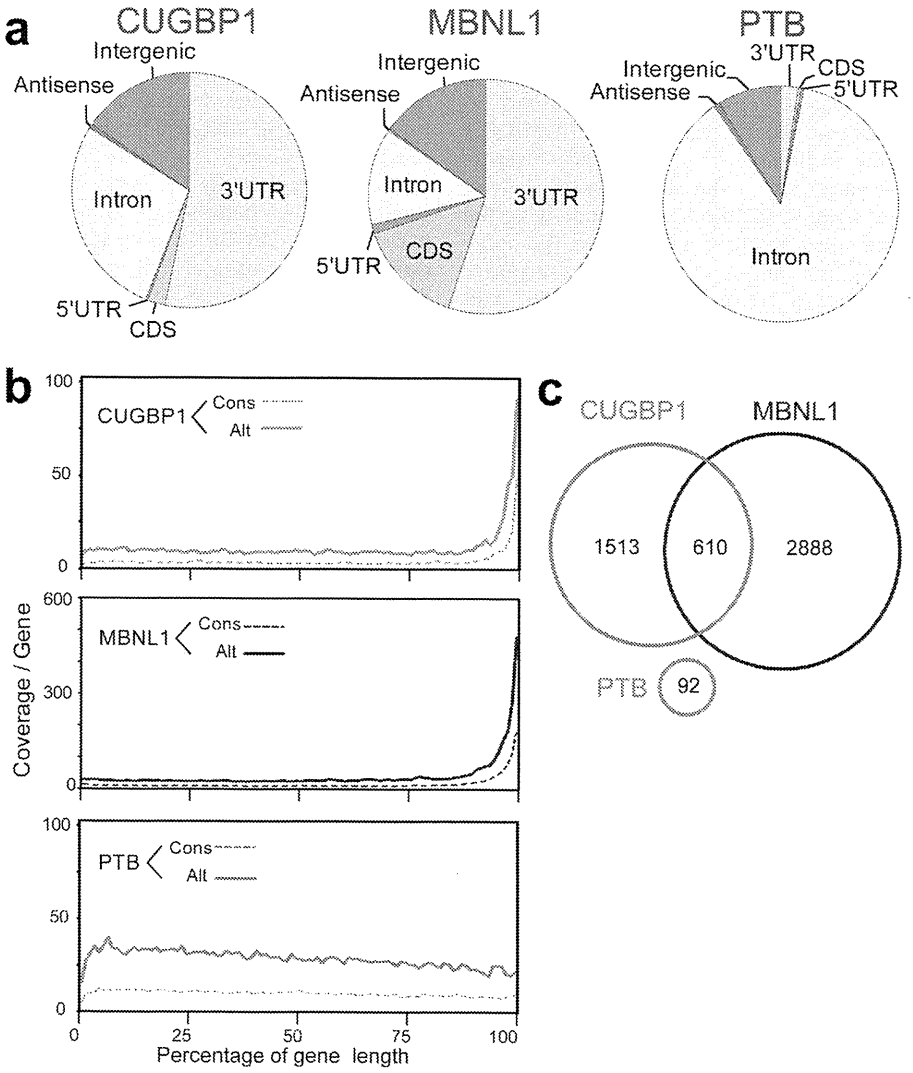

Figure 3 | Enrichment of CUGBP1 and MBNL1 CLIP-tags in the 3′ UTR. (a) Distributions of CUGBP1, MBNL1, and PTB binding regions. Binding regions are mapped to CDS (coding sequence), 5′ and 3′ UTRs, introns, intergenic regions (incl. tRNA and rRNA genes), or antisense within genes according to the UCSC knownGene annotation of the NCBI Build 37.1 mouse genome (mm9). Pie-charts show ratios of binding regions mapped to the indicated regions. (b) Distributions of CUGBP1, MBNL1, and PTB CLIP-tags mapped to the relative positions of all the mouse genes. The relative positions of the genes are shown in percentages of the gene length in abscissa. The broken lines represent 15,638 genes with constitutive transcriptional start and end sites (Cons), and the solid lines represent 7,477 genes with alternative transcriptional start or end site (Alt). (c) Venn diagram of the numbers of genes with CUGBP1-, MBNL1-, and PTB-binding regions within the 3′ UTR. Binding regions were identified using the SeqMonk software.

between these two proteins (Fig. 3c). All these data document that both CUGBP1 and MBNL1 preferentially bind to 3′ UTRs, indicating that this is a key function of both proteins in RNA processing. This suggests that the functional repertoire of MBNL1 should be expanded and that MBNL1, from being primarily regarded as regulator of alternative splicing, should also be considered as an important regulator of 3′ UTR-mediated processes, such as mRNA stability/degradation.

MBNL1 destabilize mRNAs. To analyze the function of CUGBP1/MBNL1 binding to 3′ UTRs, we made luciferase reporter constructs harboring CUGBP1/MBNL1-binding sites in the 3′ UTR. Since no CLIP tags were observed in the 3′ UTR of *Gapdh* (Supplementary Fig. S8), we made a *luciferase-Gapdh* 3′ UTR expression vector, and then inserted 12 repeats of GT and 7 repeats of CTG immediately after the stop codon of *luciferase* to introduce a CUGBP1-binding site (GU rich motif) and an MBNL1-binding site (YGCY motif), respectively (Fig. 4a). We also inserted 12 AC repeats as a control. Due to the high expression level of CUGBP1 in C2C12 cells we used HEK293 cells for transient transfection of these reporter constructs along with CUGBP1/MBNL1 expression vectors. For the constructs with *Gapdh* 3′ UTR alone or with AC repeats inserted, overexpression of CUGBP1 or MBNL1 had no effect on luciferase activity (Fig. 4b). For the GT repeat construct, overexpression of CUGBP1 decreased the luciferase activity, but MBNL1 had no effect. For the CTG repeat construct overexpression of MBNL1 dramatically decreased the luciferase activity, and also overexpression of CUGBP1 significantly reduced luciferase activity (Fig. 4b). In order to shed light on the mechanism underlying the observed decrease in luciferase activity we investigated the decay of *luciferase* mRNA. The SV40 promoter of the luciferase reporter constructs was replaced with a tet-repressible promoter, and HEK293 Tet-off cells were transiently transfected with these constructs. Doxycycline was added to the medium to stop transcription of the tet-responsive promoter, and the temporal profiles of *luciferase* and *GAPDH* mRNA levels were measured. Overexpression of MBNL1 together with the CTG repeat reporter construct resulted in highly increased decay of *luciferase* mRNA and CUGBP1 overexpression together with the GT repeat reporter construct also increased mRNA decay. Overexpression of either protein together with the *Gapdh* 3′ UTR control construct did not alter mRNA decay (Fig. 4c). These data demonstrate that binding of CUGBP1 and MBNL1 to the 3′ UTR promotes mRNA decay. To examine whether CUGBP1 and MBNL1 regulate decay of endogenous mRNAs, we next analyzed mRNA stability in actinomycin D treated C2C12 cells by expression arrays following siRNA knock down of CUGBP1 or MBNL1 (GEO accession number, GSE27583). To identify genes with reliable half-life estimates, we restricted our analysis to 195 transcripts using three conditions: (i) half-life between 2.5–5 hrs; (ii) correlation coefficient of fitting to an exponential decay greater than 0.9; and (iii) RMA-normalized signal values more than 100 at all time points. The median half-life of all the transcripts matching these criteria in the control is 3.56 hrs, whereas those from CUGBP1- and MBNL1-knocked down cells are significantly prolonged to 3.91 hrs and 3.73 hrs, respectively (Fig. 5a). We chose four additional representative mRNAs with a cluster of either CUGBP1- or MBNL1-tags in the 3′UTR, and confirmed by real time PCR that knockdown of either CUGBP1 or MBNL1 results in approximately two-fold increase in mRNA half-life of these target mRNAs (Fig. 5b). The half-lives of 100 out of 195 transcripts are prolonged both by knockdown of CUGBP1 and MBNL1, suggesting overlapping activity in the regulation of mRNA decay by CUGBP1 and MBNL1. We next analyzed the relationship between change in mRNA half-life and coverage of HITS-CLIP tags in the 3′ UTRs. We found that genes displaying prolongation of half-lives in response to CUGBP1 knockdown harbors more CUGBP1-tags in their 3′ UTRs, compared to those displaying shortening of half-lives (Fig. 5c). Similarly, genes that display prolongation of their half-lives in response to MBNL1 knockdown have more MBNL1-tags in their 3′ UTRs (Fig. 5c).

Gene Ontology analysis of CUGBP1/MBNL1-bound 3′ UTRs revealed that the terms 'cytoskeletal protein binding, 'transcription factor binding' and 'RNA binding' are significantly overrepresented for CUGBP1- and MBNL1-bound genes (Table 1).

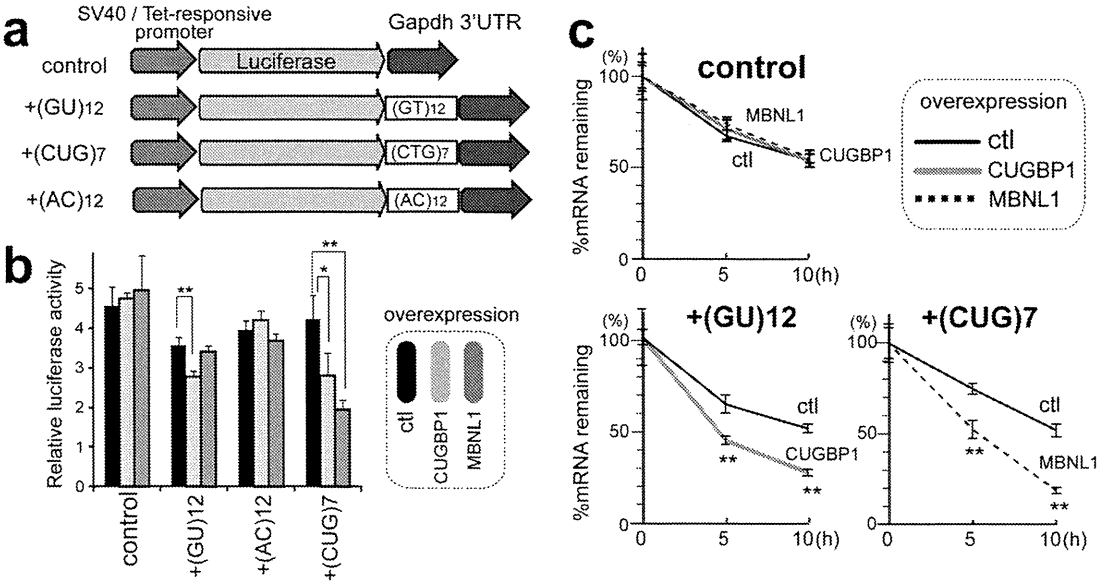

Figure 4 | Decay of *luciferase* mRNA by overexpression of CUGBP1/MBNL1. (a) Schemes of luciferase reporter plasmids harboring *Gapdh* 3′ UTR. Each construct was made carrying either SV40 or tet-responsive promoter. (b) Luciferase activity after overexpression of CUGBP1/MBNL1. HEK293 cells were transfected with the indicated SV40-driven luciferase reporter constructs. Luciferase activity is normalized for the transfection efficiency using co-transfection of pRL/SV40. (c) Decay of luciferase mRNA after overexpression of CUGBP1/MBNL1. HEK293 Tet-off cells were transfected with the indicated tet-responsive promoter-driven luciferase reporter constructs. Doxycycline was added to the medium to stop transcription at time 0. Temporal profiles of luciferase mRNA decay were quantified by real time RT-PCR and are normalized for *Gapdh* mRNA levels. All experiments were triplicated, and the mean and s.d. are indicated (* $p < 0.05$; ** $p < 0.01$).

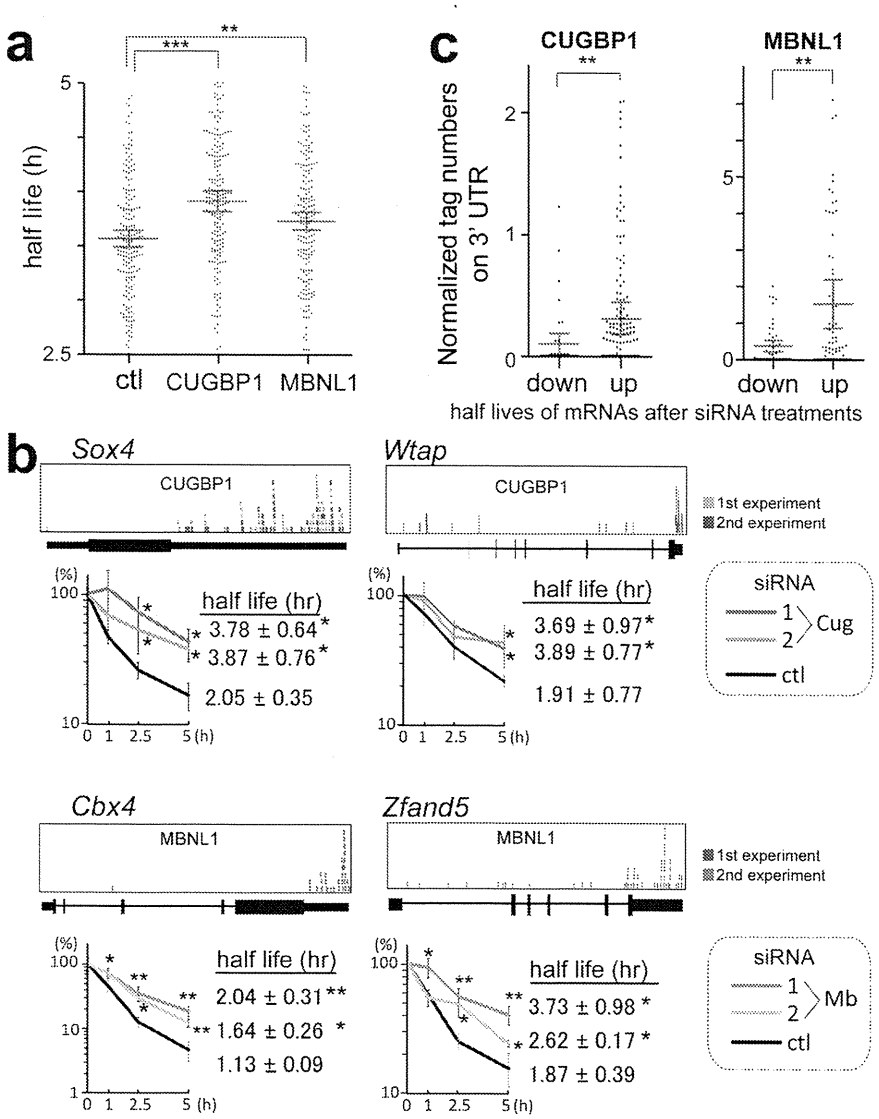

Figure 5 | Global analysis of mRNA decay by expression array of C2C12 cells treated with CUGBP1/MBNL1 siRNA. (a) Half-lives of mRNAs in C2C12 cells with the indicated siRNAs. Red lines represent means and 95% confidence intervals. ** $p < 0.01$ and *** $p < 0.001$. (b) Real-time RT-PCR analysis of the stability of four representative endogenous mRNAs, which were detected by expression arrays. CLIP-tag distributions are shown above each gene structure. C2C12 cells were treated with either control (ctl), CUGBP1 (Cug), or MBNL1 (Mb) siRNA. Actinomycin D was added to the medium to stop transcription at time 0. Temporal profiles of decay of the indicated genes were analyzed by real-time RT-PCR and are normalized for *Gapdh* mRNA levels. All experiments were triplicated, and the mean and s.d. are indicated (* $p < 0.05$ and ** $p < 0.01$). (c) Tag counts in the 3′ UTR of each gene are plotted in two categories of prolonging (up) and shortening (down) of half-lives after MBNL1 and CUGBP1 siRNAs. Red lines represent means and 95% confidence intervals. ** $p < 0.01$. Tag counts were normalized by the gene expression level at 0 h of cells treated with control siRNA.

Table 1 | The five most frequent Gene Ontology terms of mRNAs that are bound by CUGBP1 and MBNL1 to the 3′ UTR

CLIP data	GO ID	Term	P Value
CUGBP1	GO:0008092	cytoskeletal protein binding	1.58E-06
	GO:0003723	RNA binding	1.40E-04
	GO:0008134	transcription factor binding	9.65E-04
	GO:0051082	unfolded protein binding	0.003184
	GO:0019904	protein domain specific binding	0.006603
MBNL1	GO:0008092	cytoskeletal protein binding	7.31E-20
	GO:0008134	transcription factor binding	2.20E-08
	GO:0003723	RNA binding	0.001893
	GO:0019899	enzyme binding	0.002046
	GO:0032553	ribonucleotide binding	0.004210

We utilized the mRNAs that have more than 8-fold coverage of CLIP tags in their 3′UTR for the analysis by DAVID[53,54].

PITX2 is a homeobox transcription factor that regulates left-right asymmetric morphogenesis[37,38] and it is also deeply implicated in myogenesis during mouse embryonic development[39–41]. We found that the decay of *Pitx2* mRNA is prolonged by knocking down MBNL1, but not CUGBP1 in undifferentiated C2C12 cells (Fig. 6b and c). This is consistent with the fact that *Pitx2* harbors a much higher number of MBNL1-CLIP tags than that of CUGBP1-CLIP tags in the 3′ UTR (Fig. 6a). We also observed that down regulation of both CUGBP1 and MBNL1 decreases the decay of *Myod1* and *Mbnl2* mRNA, but not that of *Gapdh* mRNA (Supplementary Fig. S8). Similarly, down regulation of CUGBP1 decreases the decay of other myogenic transcription factors such as *Myog* and *Mef2a* mRNAs, and also of *Cugbp2* (Supplementary Fig. S9). Furthermore, knockdown of CUGBP1 and MBNL1 prolongs decay of *Mbnl1* and *Cugbp1* mRNAs, respectively, suggesting a mechanism for cross-regulation of expression of MBNL1, CUGBP1, and their family proteins (Supplementary Fig. S8).

To analyze more directly the role of MBNL1 binding to the 3′ UTR in regulation of mRNA decay, we examined the mRNA stability of firefly luciferase fused with the 3′ UTR of *Pitx2* (Fig. 6a). There are 11 YGCY motifs in the 3′ UTR of *Pitx2*, and 4 of the 11 motifs have MBNL1-CLIP tags. We introduced artificial mutations in these 4 motifs to prevent binding of MBNL1 (Fig. 6a). Consistent with the proposed role for MBNL1 in mRNA decay, we observe that disruption of the MBNL1-binding motifs in the *Pitx2*-3′ UTR abolished responsiveness to MBNL1 knockdown (Fig. 6d). Furthermore, immunoblots demonstrated that MBNL1-knockdown enhanced expression of endogenous PITX2 in C2C12 cells (Fig. 6e). These data suggest that MBNL1 promotes decay of *Pitx2* mRNA and thereby represses expression of the PITX2 protein.

Taken together, all of our data are consistent with a model where CUGBP1 and MBNL1 facilitate mRNA decay through binding to the 3′ UTR of target genes.

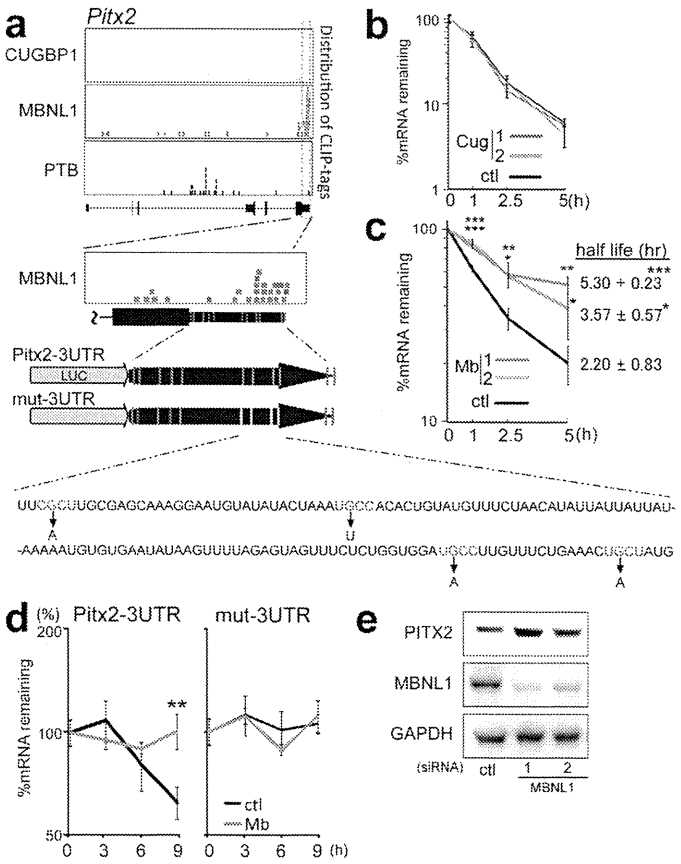

Figure 6 | MBNL1 binds to 3′ UTR of *Pitx2* and facilitates decay of *Pitx2* mRNA. (a) Distributions of MBNL1 CLIP-tags in the *Pitx2*-gene structure, and schemes of luciferase reporter plasmids harboring wild-type (*Pitx2*-3UTR) and mutated (mut-3UTR) 3′ UTRs of *Pitx2*. Red bars indicate locations of native YGCY motifs and yellow bars indicate those of mutated YGCY motifs. Individual mutations disrupting YGCY motifs are shown at the bottom. We introduced U at the 2nd YGCY motif to prevent formation of AU and AC repeats, which constitute a potential binding site of Hu proteins and hnRNP L, respectively. (b and c) Decay of endogenous *Pitx2* mRNA by siRNA-mediated knockdown of CUGBP1 (b) and MBNL1 (c). C2C12 cells were treated with either control (ctl), CUGBP1 (Cug) or MBNL1 (Mb) siRNA. Actinomycin D was added to the medium to stop transcription at time 0. Temporal profiles of decay of the indicated genes were analyzed by real-time RT-PCR and were normalized for *Gapdh* mRNA levels. All experiments were triplicated, and the mean and s.d. are indicated (* $p < 0.05$; ** $p < 0.01$; *** $p < 0.001$). (d) Decay of luciferase mRNA in the Pitx2-3UTR and mut-3UTR constructs after either control (ctl) or MBNL1 (Mb) siRNA in TetON-C2C12 cells. Culture medium was replaced by medium without doxycycline to stop transcription at time 0. Temporal profiles of luciferase mRNA decay are quantified by real-time RT-PCR and are normalized for *Gapdh* mRNA levels. All experiments were triplicated, and the mean and s.d. are indicated (** $p < 0.01$). (e) Immunoblot of PITX2 in undifferentiated C2C12 cells at 48 hrs after transfection of MBNL1 siRNA.

Discussion

CUGBP1 and MBNL1 are developmentally regulated RNA-binding proteins that are causally associated with myotonic dystrophy type 1. In this study, we show that both CUGBP1 and MBNL1 preferentially bind to 3′ UTRs and destabilize the bound mRNAs. In particular, we show that CUGBP1 and MBNL1 destabilize myogenic differentiation factors and RNA-binding proteins. In addition, our results confirm and significantly expand the current knowledge of the splicing-regulatory effects of CUGBP1 and MBNL1. Taken together, the data from the present study indicates that CUGBP1 and MBNL1 are closely related and cross regulate alternative splicing and mRNA decay.

MBNL1 binding to 3′ UTRs has not been previously reported. We show for the first time that MBNL1 binds to 3′ UTRs and promotes mRNA decay in both artificial constructs and in endogenous genes. We also demonstrate by expression arrays that both CUGBP1 and MBNL1 facilitate mRNA decay by binding to 3′ UTRs. The present study demonstrates global *in vivo* interactions between CUGBP1 and 3′ UTRs and reveals that CUGBP1 also preferentially binds to 3′ UTR rather than exons/introns. We provide *in vivo* evidence that CUGBP1 facilitates mRNA decay of a broad spectrum of genes in addition to the previously reported genes[25–27,42–44].

Interestingly, we find that MBNL1 promotes decay of *Cugbp1* mRNA and that CUGBP1 promotes decay of *Mbnl1* mRNA, and that this is associated with corresponding changes at the protein level during differentiation of C2C12 cells (Supplementary Fig. S4b). This may suggest that expression of CUGBP1 and MBNL1 are mutually regulated in myogenic differentiation. Kuyumcu-Martinez and colleagues report that expanded CUG repeats of *DMPK* through an unknown mechanism leads to phosphorylation and thereby to stabilization of CUGBP1 in DM1 myoblasts[10]. Our studies additionally suggest that loss of MBNL1 in DM1 could lead to decreased decay of *CUGBP1* mRNA and hence to further increase of CUGBP1 activity. Although CUGBP1 is not upregulated in adult MBNL1-knockout mice, this mechanism could lead to increased misregulation of splicing and decay of the mRNAs of target genes in embryonic development that culminates in the DM1 phenotype.

We find that binding sites for CUGBP1 and MBNL1 are enriched around alternative cassette exons (Fig. 2a). The binding sites for CUGBP1 are prominent in adjacent intronic regions flanking alternative exons. Our functional analysis reveals that binding of CUGBP1 to the upstream intron facilitates exon skipping, whereas